



SAE Aero Design East, 2022

School Name: Dwarkadas J. Sanghvi College of Engineering

Team Name: DJS SKYLARK - MICRO CLASS

Team Number: 311

Team Members

Team Captain: Tanmay Kshire

Abhishek Malichkar
Aditya Bhalerao
Aditya Suri
Anushka Shah
Ardon Kotey
Arshish Balaporia
Arya Raut
Aryan Ashar
Deep Dholakia
Hariaksh Pandya

Harshal Soni
Het Shah
Hetavi Mehta
Joel Ponmany
Krish Morabiya
Malay Thumbar
Manthan Mistry
Mrunmay Mhapankar
Nimish Sabnis

Parv Khandelwal
Radhika Jethwa
Rayaan Juvale
Shlok Mandloi
Shubham Modi
Siddhi Tamanekar
Tejas Pathak
Vighnesh Patil

STATEMENT OF COMPLIANCE

Certification of Qualification

Team Name	DJS Skylark - Micro Class	Team Number	311
School	Dwarkadas J. Sanghvi College of Engineering		
Faculty Advisor	Prof. Shashikant Auti		
Faculty Advisor's Email	shashikant.auti@gmail.com		

Statement of Compliance

As faculty Adviser:

SMA (Initial) I certify that the registered team members are enrolled in collegiate courses.

SMA (Initial) I certify that this team has designed and constructed the radio-controlled aircraft in the past nine (9) months with the intention to use this aircraft in the 2022 SAE Aero Design competition, without direct assistance from professional engineers, R/C model experts, and/or related professionals.

SMA (Initial) I certify that this year's Design Report has original content written by members of this year's team.

SMA (Initial) I certify that all reused content have been properly referenced and is in compliance with the University's plagiarism and reuse policies.

SMA (Initial) I certify that the team has used the Aero Design inspection checklist to inspect their aircraft before arrival at Technical Inspection and that the team will present this completed checklist, signed by the Faculty Advisor or Team Captain, to the inspectors before Technical Inspection begins.



Signature of Faculty Advisor

04/09/22

Date



Signature of Team Captain

4/4/2022

Date



Table of Contents

List of Figures, Tables, Symbols, and Abbreviations	2
1.0 Executive Summary	3
1.1 System Overview and Discriminators	3
1.2 Understanding Requirements	3
1.3 Competition Projections	4
2.0 Project Management	4
2.1 Schedule Summary	4
2.2 Personnel Management	5
2.3 Cost Report	5
2.4 Risk Analysis	6
3.0 Design Layout and Trades	6
3.1 Overall Design Features and Details	6
3.2 Competitive Scoring Strategy and Analysis	8
3.3 Design Derivations	13
3.4 3-D Printed Interfaces and Attachments	16
4.0 Loads, Environments and Assumptions	16
4.1 Design Load Derivations	16
4.2 Environmental Considerations	17
5.0 Analyses	18
5.1 Analytical Tools	18
5.2 Developed Models	19
5.3 Performance Analyses	19
5.3.1 Dynamic Thrust Performance	19
5.3.2 Take-off and Climb-out Performance	20
5.3.3 Flight and Maneuver Performance	20
5.3.4 Static and Dynamic Stability	21
5.3.5 Aircraft Performance Prediction	21
5.3.6 Drag Polar Analysis	22
5.4 Structural Analyses	22
5.4.1 Critical Margins	22
5.4.2 Applied Loads and Material Selection	22
6.0 Sub-Assembly Tests and Integration	24
7.0 Manufacturing	25
8.0 Conclusion	25
Appendix A – Backup Calculations	26
Appendix B – Technical Data Sheet	
2D Drawing	



List of Abbreviations

CG	Center of Gravity	TMA	Tail Moment Arm
FoS	Factor of Safety	CAD	Computer Aided Drawing
MoS	Margin of Safety	CFD	Computational Fluid Dynamics
UTM	Universal Testing Machine	AR	Aspect Ratio

List of Symbols

C	Chord of Control Surface	S_{TO}	Take-off Distance
C_D	Drag coefficient of Aircraft	T_d	Dynamic Thrust
C_{DI}	Lift-Induced Drag Coefficient	T_s	Static Thrust
C_{D0}	Zero-Lift Drag Coefficient	v	Airspeed
C_f	Skin Friction Drag Coefficient	v_d	Dive speed
C_L	Lift Coefficient of Aircraft	v_E	Aircraft Equivalent speed
C_M	Coefficient of Moment	v_{gE}	Gust Equivalent Speed
h_n	Distance: Wing Leading Edge to Neutral Point	V_{TO}	Velocity Required to Take-off
k_g	Gust Alleviation Factor	V_{Stall}	Stall Speed of Aircraft
L	Lift	v_x	Velocity of Aircraft in x-direction
m	Mass of the Aircraft	v_y	Velocity of Aircraft in y-direction
n	Load Factor	\bar{V}	Volume Tail Coefficient
S	Wing Planform	α	Angle of Attack
S_1	Maximum Control Surface Deflection	ω	Frequency
S_2	Maximum Servomotor Deflection	Φ	Aircraft Bank Angle

List of Figures and Tables

Figure 1(a)	System Overview and Discriminators	Figure 4(c)	Environmental Considerations
Table 1(b)	Subsystem Details	Chart 5(a)	Developed Models
Figure 2(a)	Schedule Summary	Figure 5(b)	Dynamic Thrust Performance
Figure 2(b)	Schedule and Cost Breakdown	Figure 5(c)	Take-off and Climb-out Telemetry
Table 2(c)	Risk Analysis and Mitigation	Table 5(d)	Post Flight-Test Optimization
Figure 3(a)	Wing Layout	Figure 5(e)	Minimum Turning Radius
Figure 3(b)	Fuselage Layout	Figure 5(f)	Maximum Banking Angle
Figure 3(c)	Empennage Layout	Table 5(g)	Stability Response
Figure 3(d)	Electronics System Layout	Figure 5(h)	Short Period and Phugoid Modes
Figure 3(e)	Planform Analysis	Table 5(i)	Lateral Stability Eigenvalues
Figure 3(f)	Trial Prototypes' Philosophy Selection	Figure 5(j)	Drag Polar Analysis
Figure 3(g)	Aircraft Configuration Analysis	Table 5(k)	Material Analysis
Figure 3(h)	Weibull Curve	Figure 5(l)	Crosswind Analysis
Figure 3(i)	Score vs Windspeed	Figure 5(m)	Composite Stress Analysis
Figure 3(j)	Delivery Box Biplane Analysis	Figure 5(n)	Weight Buildup
Figure 3(k)	C_M vs Alpha	Figure 6(a)	Novel Wind Tunnel Setup
Figure 3(l)	Motor-Propeller Combinations	Table 6(b)	Servo Torque Requirements
Figure 4(a)	V-n Diagram	Chart 7(a)	Manufacturing Process
Table 4(b)	Landing Shock Calculations		

1.0 Executive Summary

1.1 System Overview and Discriminators

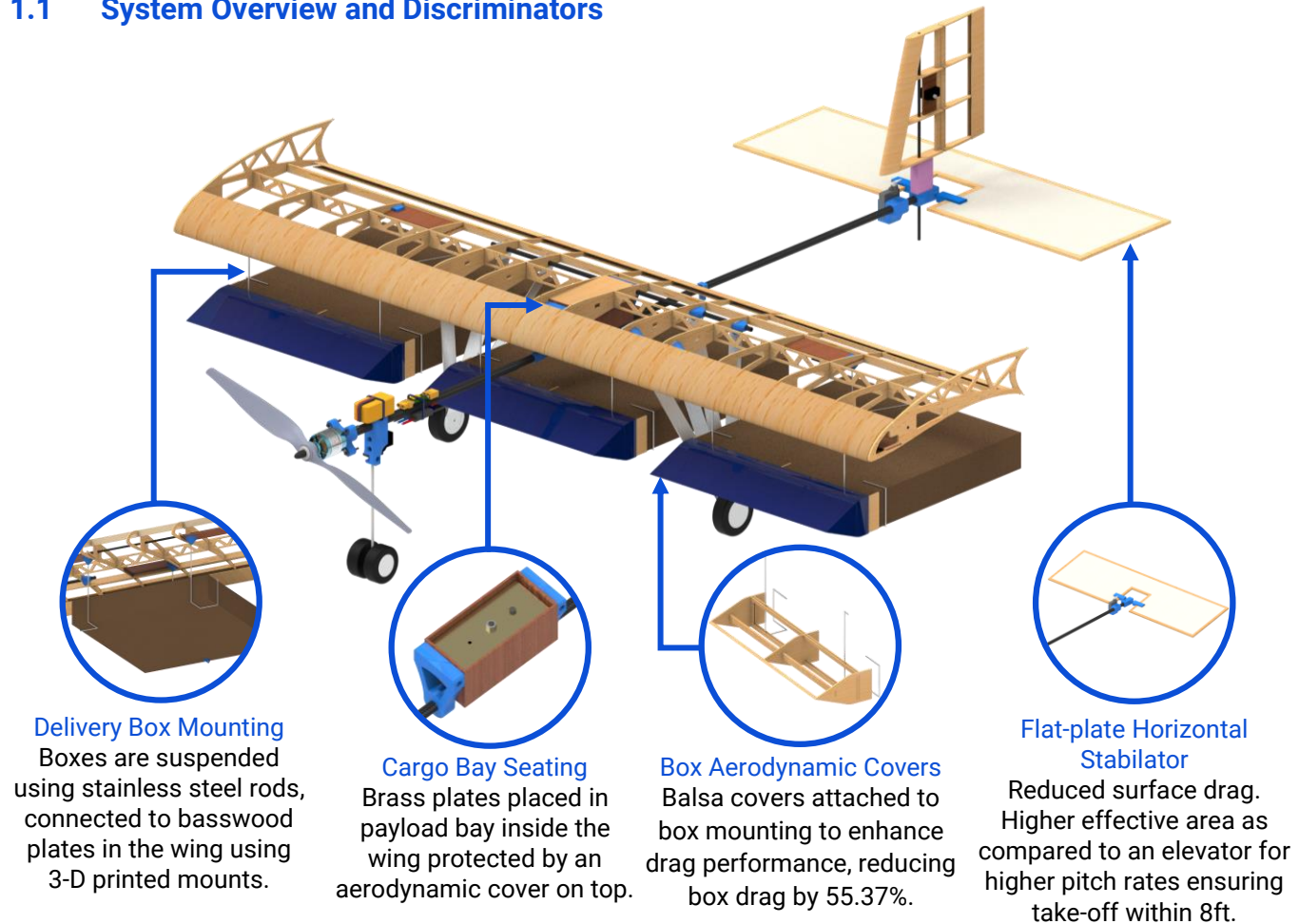


Figure 1(a): System Overview and Discriminators

Avionics	Motor	Propeller		Battery
	SunnySky X3120-7 760Kv	APC 15x8E		Dinogy LiPo 850mAh 4S
Wing	Airfoil	Span	Aspect Ratio	Planform
	S1223RTL	48 in.	4	Rectangular
Empennage	Horizontal Tail Airfoil	Vertical Tail Airfoil		Configuration
	Flat-Plate	NACA0009		Inverted T-Tail
Scoring Strategy	Delivery Boxes	Time Taken to 300ft. (sec)		Payload Plates (lbs.)
	3 Large Boxes	8.1		3

Table 1(b): Subsystem Details

1.2 Understanding Requirements

The team gained a thorough understanding of the problem statement, deducing several variables to be mutually interdependent, of which time was found to rely upon multiple ungovernable factors. Hence, the team employed a probabilistic approach, performing simulations and empirical testing, to further shape design decisions.



1.3 Competition Projections

The team designed the aircraft to carry 3.938lbs. of total cargo weight, comprising 3 Large Delivery Boxes and 3lbs. of Payload Plates in 8.1 seconds, achieving a projected score of 32.004 points per round and 96.012 points in total. Combining our flight scores with strong Design Report and Technical Presentation scores, we aim to place in the Top 3 Overall. We obtained these scores by performing in-depth analyses on the scoring equation and empirical testing to understand which parameters to optimize, based on their impact on the score. This was followed by extensive trade studies for components based on the analytical results obtained.

2.0 Project Management

2.1 Schedule Summary

The COVID-19 pandemic and the resulting curfews in India heavily affected the team's schedule throughout the year. The team began work in September as the restrictions were relaxed until when, we trained recruits and researched different designs and ideas. We based our timeline on cycles of design, testing and optimization, working around our exam schedule. We built five trial prototypes, empirically testing design and scoring philosophies. Three development prototypes were built upon the selected philosophy. With each, we introduced a slew of improvements which saw an increase in score and scoring consistency (**Section 5.3.2**).

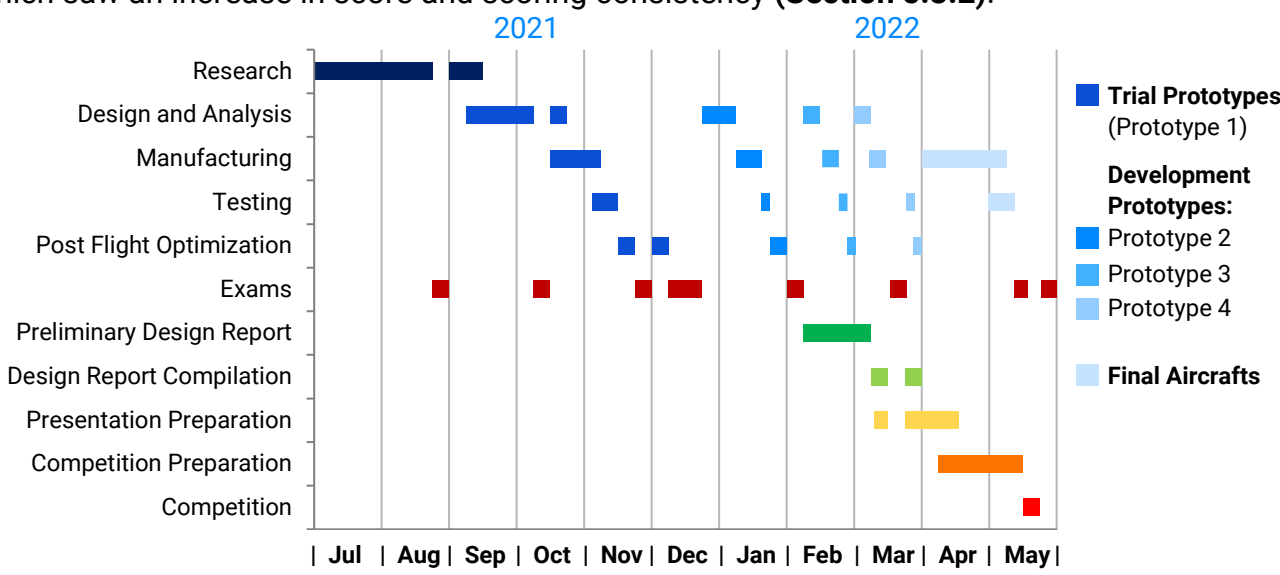


Figure 2(a): Schedule Summary

2.2 Personnel Management

Comprising of 28 students, the team was segregated into aerodynamics, structures and stability, avionics, and marketing departments. This ensured that ideas could be shared and discussed effectively inter and intra-departmentally allowing for the efficient execution of the schedule mentioned above. Over time, the Design Report and Technical Presentation groups were formed.

2.3 Cost Report

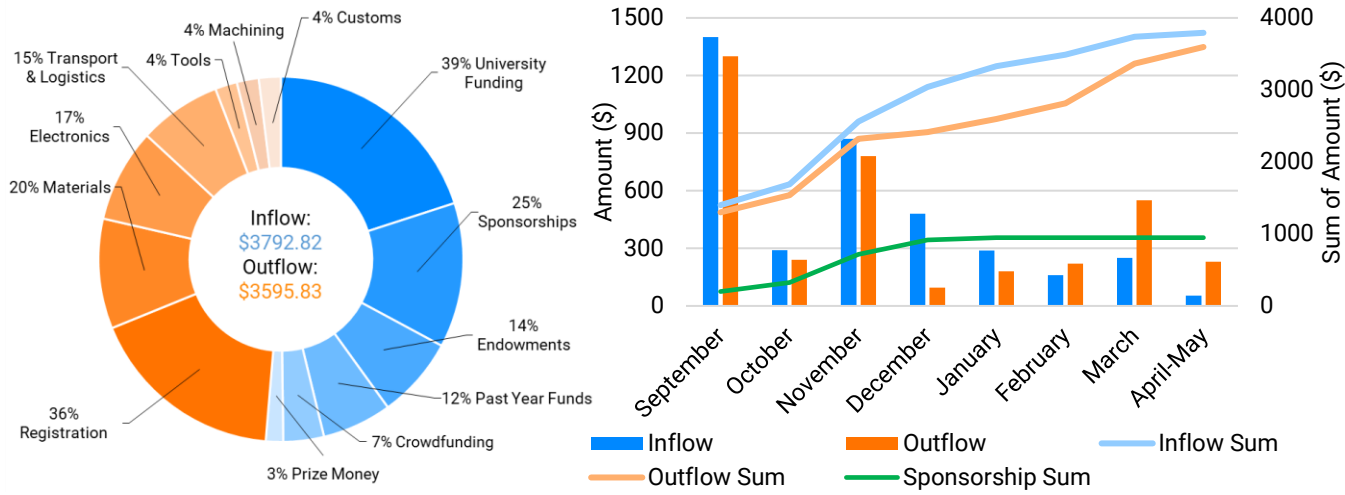


Figure 2(b): Schedule and Cost Breakdown

COVID-19 heavily affected the team's inflow of funds, starting with delayed university funding, reduced crowdfunding, and cancellation of the annual aero-modeling workshop that the team conducts to raise funds. The marketing department generated 167% more funds through sponsorships as compared to last year. These additional funds were used to manufacture and test radical design philosophies. The outflow of funds largely comprised of electronic components, raw material procurement, registration fee, tools, and logistics. To reduce the high material procurement costs, we contacted international wholesalers directly. High customs duties, long shipping periods, and worldwide product shortages limited our options for testing electronics, which we overcame by using online tools and simulations to shortlist components. Figure 2(b) represents how funds were managed through the year to eliminate any financial blockages in the design process and manufacturing.



2.4 Risk Analysis

Risk Factor	Mitigation	Outcome
COVID - 19 Pandemic	Team Vaccination; Frequent RT-PCR Tests; Stagger Members for Manufacturing; Double masking; Workshop Sanitization.	26/28 members COVID negative over the year; 92.85% negativity rate.
Structural Component Failure	Use high tensile strength materials (Figure 5(m)); Assemble structures with strong bonding agents and cyanoacrylates.	Increased structural reliability and reduced failure rate to 1/10 flight rounds.
Material Acquisition Delays	Use materials & components sparingly; Order materials in timely cycles; Wholesale Orders	Material available in urgency; No delays in manufacturing; Lowered Costs
Monetary Constraints	Sponsorships; Crowd funding; Acquire funds through member contributions. (Section 2.3)	Spare funds for emergencies; Ensured uninterrupted operations of the team
High Impact Landing Shocks	Use wing mounted Aluminum main landing gear connected to CF spars and stainless-steel nose landing gear. (Section 3.3.5)	All impulsive loads absorbed by the CF tube; No failure of airfoil ribs in 10/10 full payload flight rounds.
Box Flutter and Damage	3-point contact mounting structure; Adequate ground clearance for boxes. (Section 3.1.3)	Box flutter eliminated and no box damage observed in extensive testing.
Crosswinds and Gusts	Minimize longitudinal sectional area & optimize rudder performance. (Figure 5(l))	Smoothen flight trajectory; Immediate corrections to adverse yaw motions.
Servo & Control Surface Failures	Endurance testing performed on servos.	No flight crashes due to servo failures.



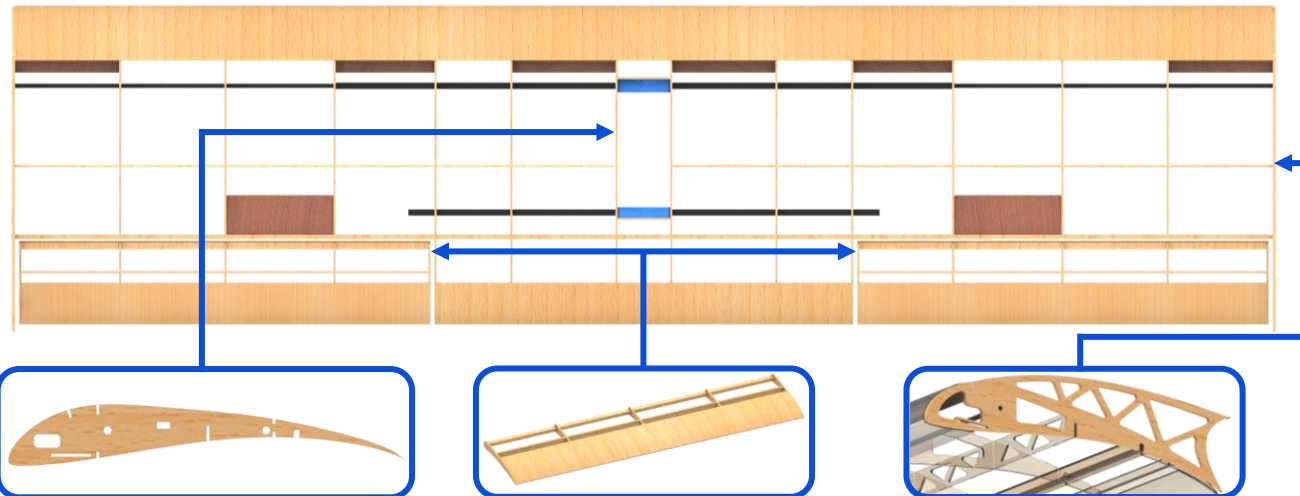
Impact (High/Med)

Table 2(c): Risk Analysis and Mitigation

3.0 Design Layout and Trades

3.1 Overall Design Features and Details

3.1.1 Wings



Airfoil Shaped Ribs

S1223RTL with chord 12", made from 2mm thick balsa to reduce FoS and empty weight. Weight reductions implemented.

Aileron

Covers 17.50% of wing area to produce high rolling moments. Placed outside the propwash region for increased effectiveness.

Shark-fin Winglet

Increases effective wing area, leading to reduced wingtip vortices and a 15.38% increase in lift.

Figure 3(a): Wing Layout

The team opted for a rectangular planform choosing airfoil the S1223RTL with the maximum wingspan of 48". The wing is made of airfoil-shaped ribs, constrained using balsa jigs and two hollow co-axial CF main spars to sustain in-flight loads while maintaining a low empty weight.

The wing is attached to a single cylindrical twill weave CF boom using 3-D printed mounts.

3.1.2 Fuselage and Landing Gear

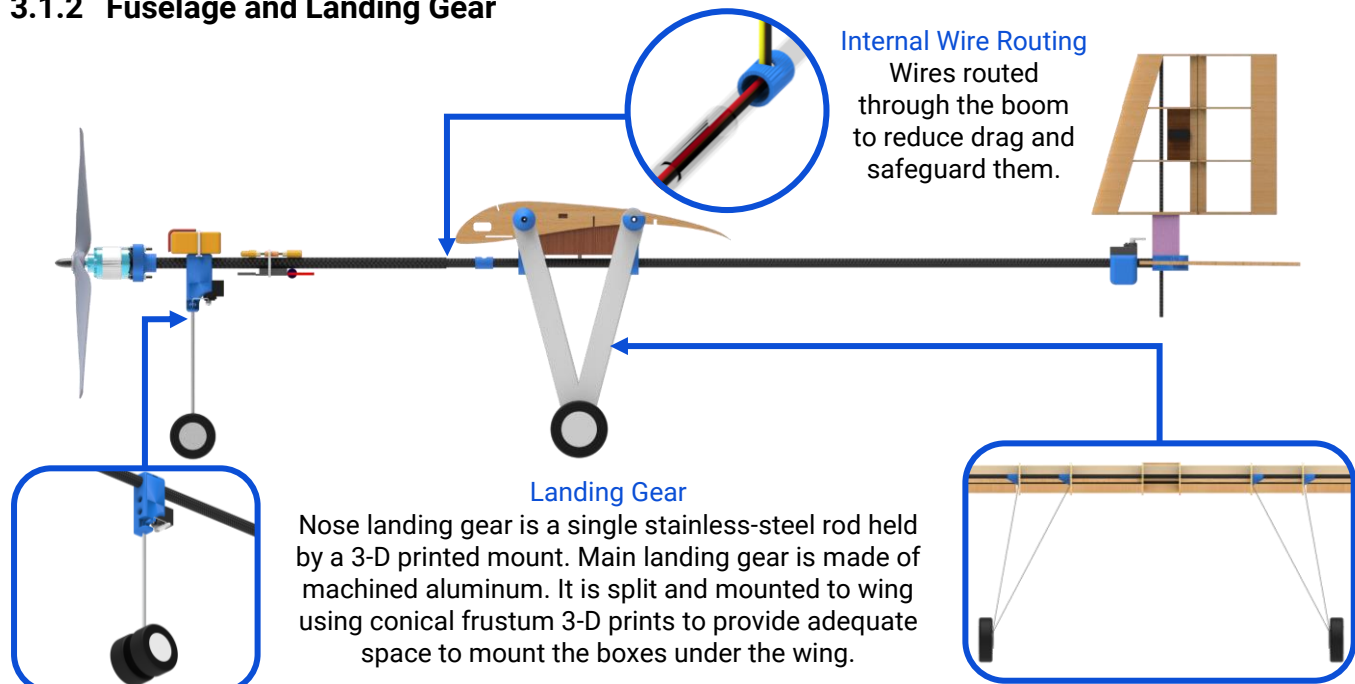


Figure 3(b): Fuselage Layout

The boom structure comprises of two co-axial twill weave CF tubes of diameters 12 and 10mm, connected to the motor, battery, wings, and tails using 3-D printed connectors. It is 48.17% lighter than a conventional fuselage, reducing drag by 42.68%. We used a tricycle landing gear owing to its immunity to ground looping and its ability to let the tail overhang from the platform, enabling efficient use of the 8ft. take-off distance.

3.1.3 Delivery Boxes and Payload

The team machined 3 lbs. of brass plates (4" x 1.8" x 0.118") and placed them near the calculated empty CG [Section 5.4.2 3) B.] ensuring its proximity to the overall CG. The cargo bay, made of basswood, is constrained laterally by the wings and longitudinally by the 3-D printed wing mounts. This facilitates unloading in 25 seconds, and loading in under 1 minute, to allow frequent flights in the newly introduced Round-less system. Efficient packaging, ease of loading and machinability of brass plates were given priority, with the top of the cargo bay recessed from the suction surface of the wing to reduce drag. The 3 Large Boxes are individually constrained using a 3-point contact system to eliminate box flutter and facilitate connection to the wing.

3.1.4 Empennage

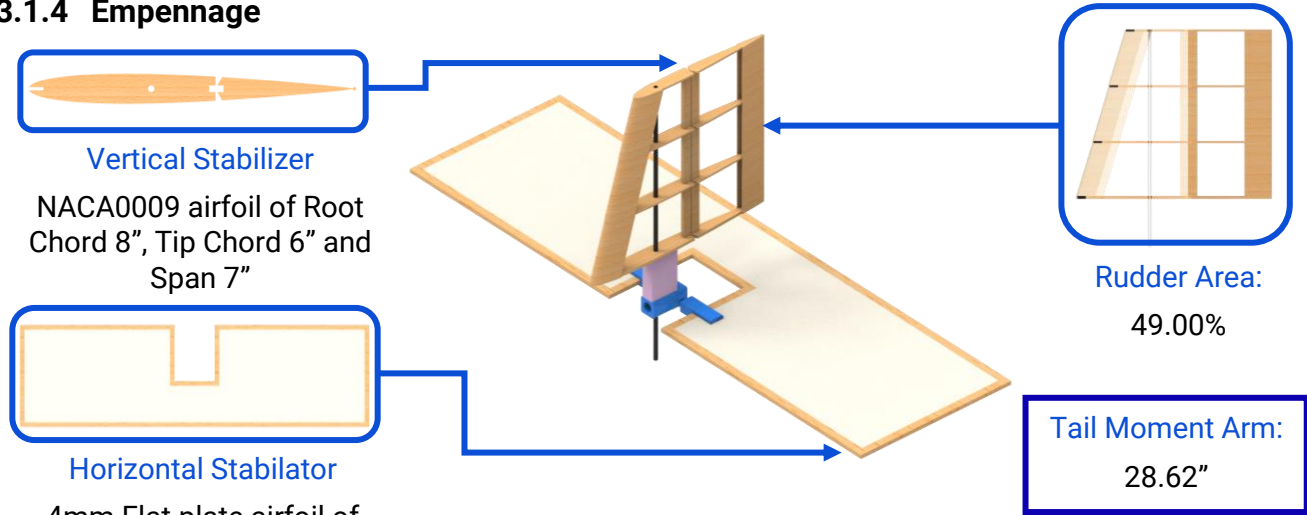


Figure 3(c): Empennage Layout

The aircraft utilizes an inverted T-Tail configuration for its reliability while reducing empty weight by 34% as compared to a U-Tail. We decided to use the horizontal stabilator as a control surface, giving us higher pitching moments compared to a conventional elevator (**Section 3.3.3**). A CF tube was used as the primary spar for both, the vertical stabilizer and horizontal stabilator.

3.1.5 Avionics

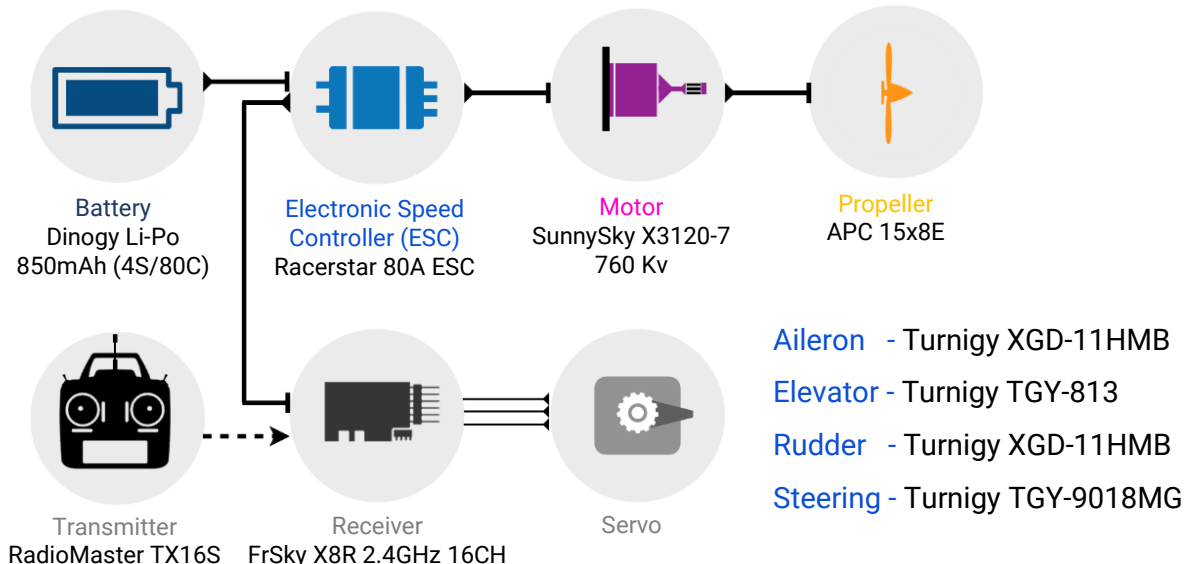


Figure 3(d): Electronics System Layout

3.2 Competitive Scoring Strategy and Analysis

The scoring equation has 3 primary variables, all mutually interdependent. These are further dependent on certain secondary variables like cargo configuration, propulsion system, and wing planform. As a result, adopting a brute force methodology, and varying all parameters

simultaneously is theoretically possible, yet practically infeasible. Thus, we performed analyses observing how varying a single secondary variable, while keeping others constant, affects the primary variables. Initially, variation of cargo configuration was rejected, since there are myriad possible configurations, each requiring structural and aerodynamic data to analyze. We varied wing planforms, as it provides tangible information on how the primary variables are affected. Optimal propulsion systems for each wingspan in Section 3.2.1 were chosen based on the team's past experience with designing and testing aircraft for spans in the range of 24" – 48".

3.2.1 Planform-Time Sensitivity Analysis

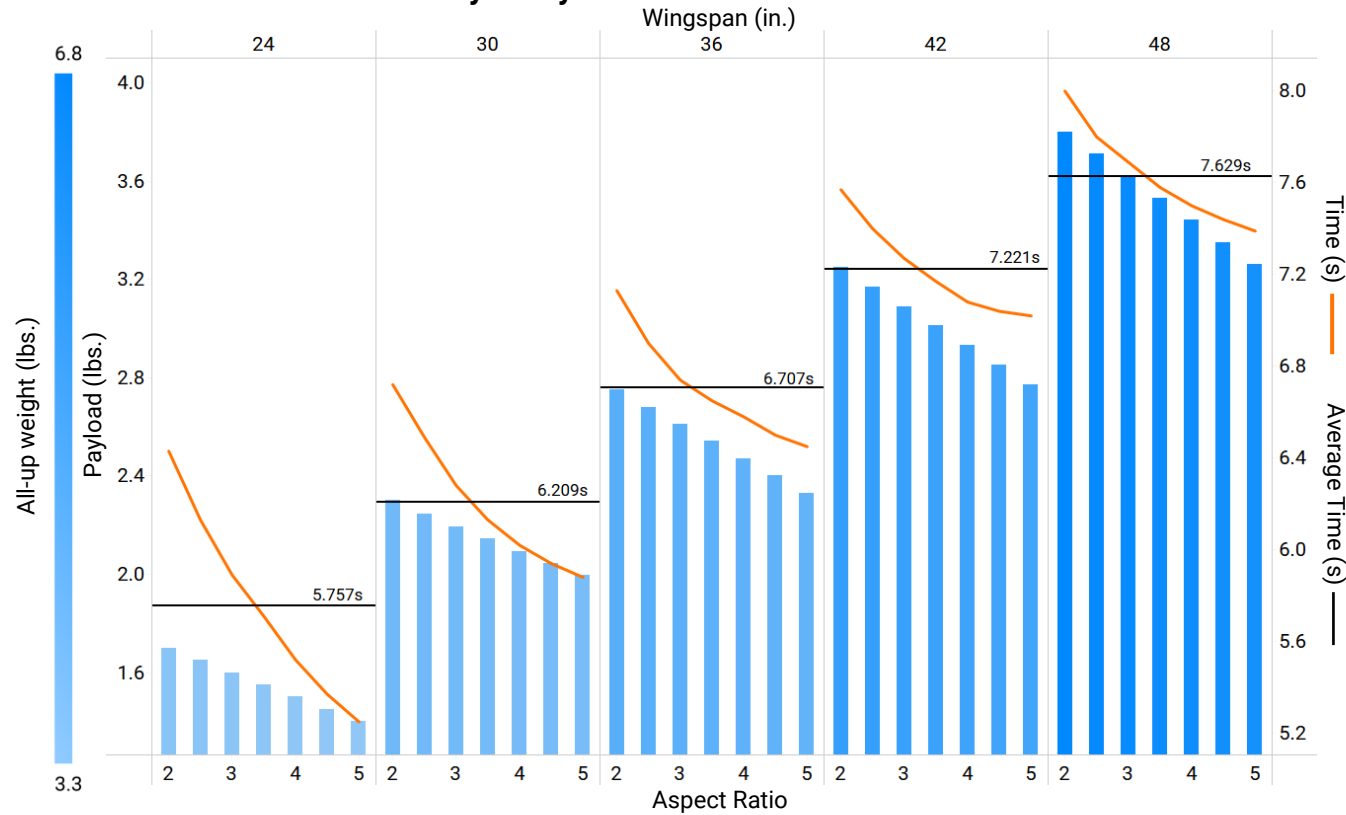


Figure 3(e): Planform Analysis

We curated a database of multiple airfoils to maximize lift, airfoil efficiency, and stall angle, while minimizing drag. Of these, S1223RTL was found to perform the best when run on Tornado VLM Solver for a fixed set of wing planforms. We then ran low-mesh CFD analyses performing an exhaustive search in the domain of over 750 wing planforms with varying dimensions (**Section 5.2**). Delivery boxes influence the drag and lift of the aircraft, thus we performed planform analyses without any delivery boxes to analyze only the effect of wing planforms on the primary

variables. Ignoring empty weights in these calculations biases the system towards higher spans. The top 10% scoring (Bonus: 0.5) configurations, as illustrated, of each span were shortlisted, negating the bias. High-mesh CFD analyses were run on these for more accurate results. We factored in the empty weight increase for wingspans by calculating the quantity of balsa by evaluating mass properties provided by our CADs and adhesives used. Lift and Drag values obtained were used as inputs to our model (**Section 5.2**). The slope of time flattens with increasing AR and the gradient of time flattens with increasing span. Thus, variance of time with aspect ratios decreases as span increases. We divided wingspans into 3 speed tiers: Fast, Medium and Slow; based on average time to 300ft. To further optimize planforms within each tier, we analyzed interpolations of NACA0012-S1223RTL from 0-100% with a step of 10%. Slow fliers performed best with NACA0012 interpolations of 0-10%, Medium fliers with 20-30% and Fast fliers with 40-50%.

3.2.2 Trial Prototypes' Analysis

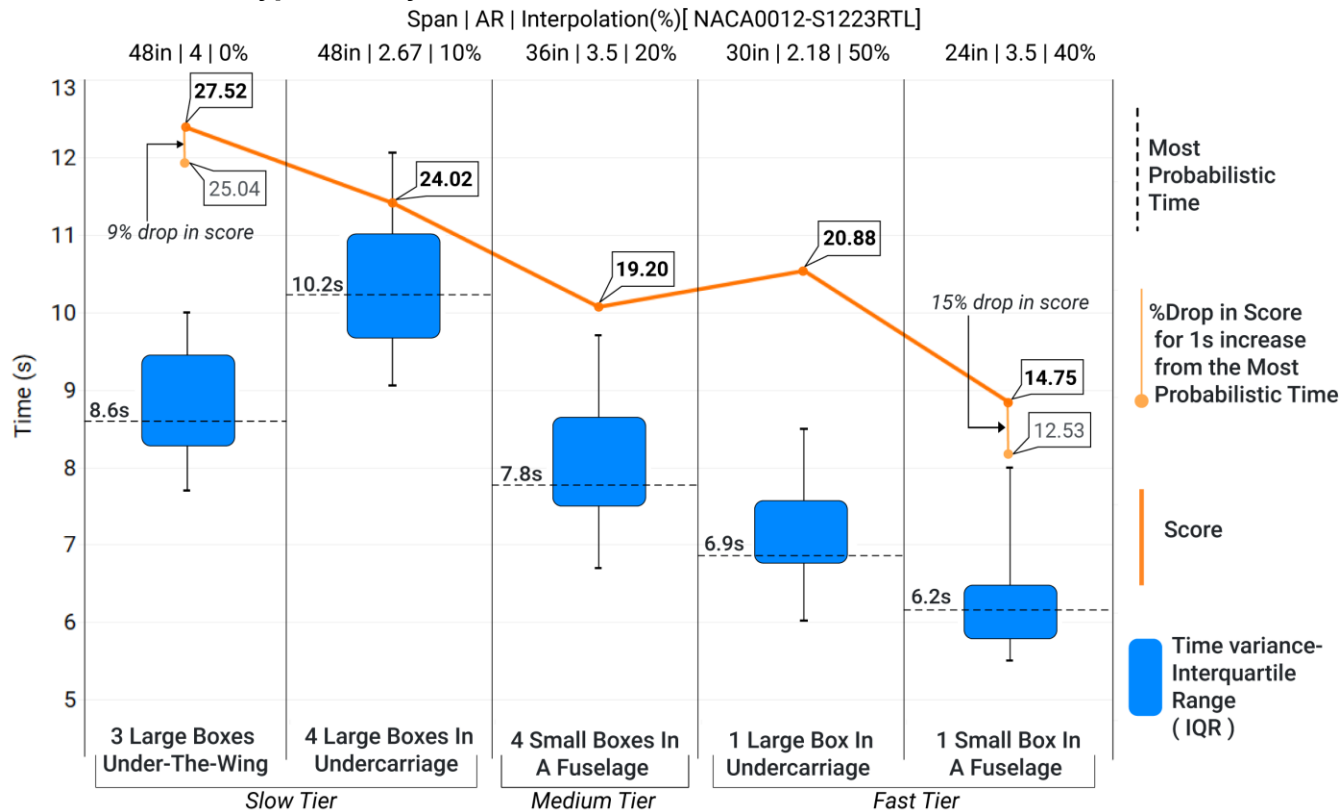


Figure 3(f): Trial Prototypes' Philosophy Selection

We explored 3 design philosophies; Cropped Delta Wing with Undercarriage, Conventional Wing



with Fuselage and No Fuselage with Under-the-Wing boxes, each providing certain inherent benefits. Box type was decided for each philosophy according to their wetted area. We performed high-mesh CFD analyses for 1-6 large boxes for the Undercarriage and 1-8 small boxes for the Fuselage with the limitation being increased empty weight, limited all-up weight and cargo bay constraints. Analyses performed for the Under-the-Wing boxes ranged from 1-4 large boxes, limited by the span. Results were segregated into the predefined speed tiers (**Section 3.2.1**), updating them based on configurations. The wind tunnel provided us with thrust values which aided us in selecting optimal propulsion system for each configuration. The top 5 scoring configurations were tested empirically, incrementing payload to find the global maxima of the score. 15 extensive flights were conducted for each configuration for the derived payload. This data was then plotted along with the score for the most probabilistic time. The IQR represents 50% of the data obtained during these flights. The bottom whisker represents an ideal flight round and top-most whisker shows maximum time taken due to presence of ungovernable factors such as crosswinds, gusts and pilot inputs. Fast and Medium fliers were eliminated due to low scores and higher %drop in scores for unit increase in time. Amongst Slow fliers, Under-the-wing was opted due to lower probabilistic time and higher score consistency.

3.2.3 Aircraft and Cargo Configuration Analysis

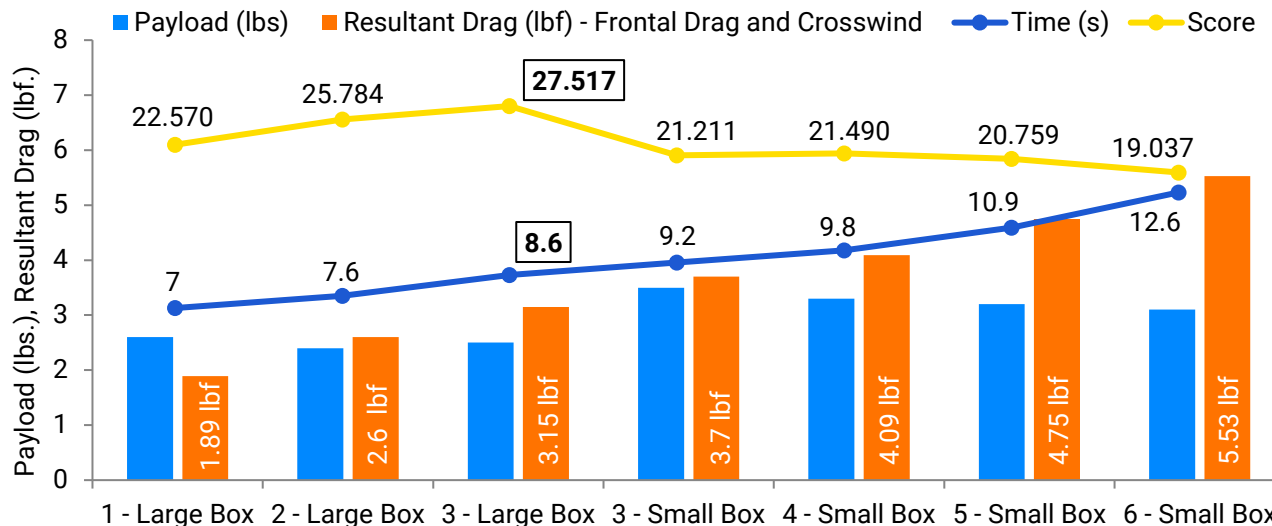


Figure 3(g): Aircraft Configuration Analysis

We built upon the results obtained in the previous section and delivery box analysis (**Section 3.2.5**), mapping delivery box configurations to the 48" span and 4 AR wing planform, using under-the-wing mounting for boxes. We also tested 0, 1 & 2 Large Boxes in the empirical tests to build a regression model ($R^2 = 0.965$), relating box layout and time taken to 300ft. Time, empty weight and take-off distance reduction being paramount, mixed delivery box strategy was eliminated as it would lead to two different kinds of mountings, thus increasing empty weight and drag. We plotted the configurations against Payload, Resultant Drag, Time Taken and Score. Small box strategies were eliminated due to high resultant drag and low scores. We selected the 3 Large Box Under-the-wing configuration on the basis of score, a biplane-like effect that increased lift (**Section 3.3.1**) and scope for drag improvements.

3.2.4 Time-Score Sensitivity Analysis

The team plotted a Weibull Distribution for windspeeds and gusts in the third week of May taking into account data from the last 5 years. The mean windspeed is found to be 4.48 ft/s, with the most probable windspeed being 2.93 ft/s. We plotted the Modelled, Empirical (Mumbai) and Predicted (Fort Worth) performance of our aircraft with scores against the range of possible winds. The configuration is found to perform optimally within 2 standard deviations, making it more resistant to external factors such as crosswinds and varying pilot inputs.

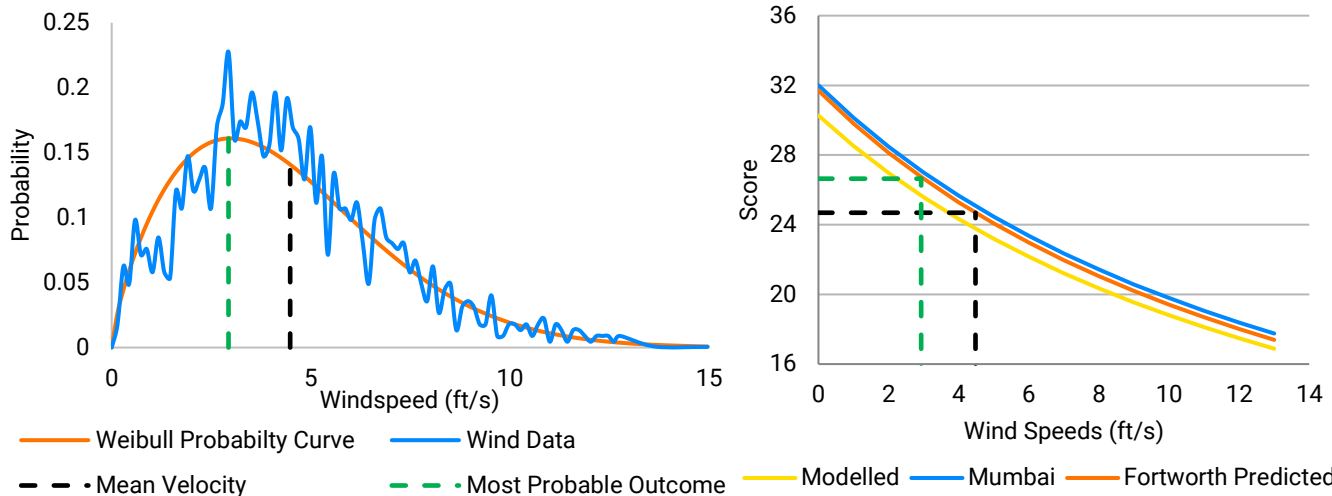


Figure 3(h): Weibull Curve

Figure 3(i): Score vs Windspeed

3.2.5 Delivery Box Trade Analysis

All above configurations come with an associated drag due to the boxes' large rectangular frontal areas. When made to sit on their largest side, both types of boxes have equal longitudinal section and frontal areas (24 in^2). The large box's slender shape and height of 2" reduces wake region, while having four times the bottom area of the small box allows it to have a significant aerodynamic advantage. The mounting of large boxes under the wing induces a bi-plane like effect (**Section 3.3.1**) with the boxes performing as exaggerated flat-plate airfoils providing a lift increase of 41.5%. The aerodynamic covers reduce associated box drag by 1.24 lbf. and time taken to 300ft by 0.2s. The final aircraft configuration selected is a wing planform of Span 48" and Chord 12", 3 Large Delivery Boxes, 3 lbs. of Payload Plates scoring 32.004 points per round.

3.3 Design Derivations

3.3.1 Wings

The team built 4 prototypes (including trial), testing high-lift devices, planforms, and mountings. The first prototype was built with a 48" span and 15"x9" chord tapered wing planform to have a compromise between payload lifted and time. The second prototype in contrast was built to increase lift by 12.85% using 48"x12" wing planform and increasing Gap of the boxes. A chord of 12" allows us to mount large boxes underneath the wing without significantly hampering

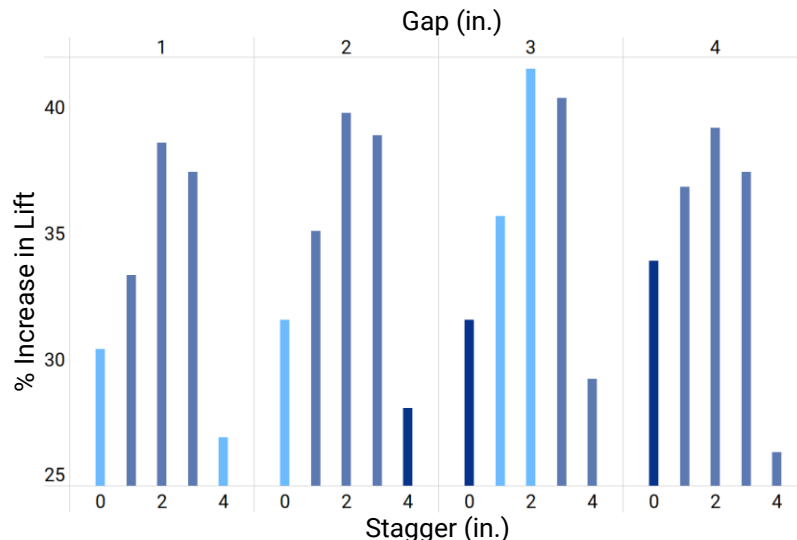


Figure 3(j): Delivery Box Biplane Analysis

downwash. We built upon the same planform in the 3rd and 4th prototype, reducing the FoS by 9.77%. With the boxes generating a biplane like effect, we optimized its mounting location by running



CFD analyses varying the Gap, Stagger and Decalage (**Figure 3(j)**). This was done in order to optimize box placements. 4" gap was rejected for lack of ground clearance. We tested the 3" gap and increased it to 3.2" to allow for clean airflow under the ailerons. The selected configuration is a 3.2" gap, 2" stagger and no decalage.

3.3.2 Vertical Tail (VT)

The requirements for yawing were 14.5% lower than first calculated after extensive flight testing, due to a small longitudinal section. Thus, we chose a conventional tail design for its low empty weight. We sized the tail by computing the required tail volume coefficient (0.047), analyzing crosswinds at Fort Worth. NACA0009 was selected for its low drag at 0° angle of attack.

3.3.3 Horizontal Tail (HT)

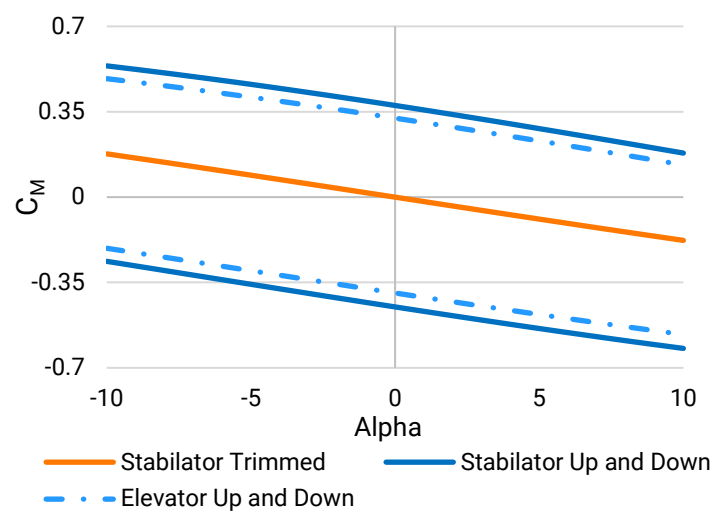


Figure 3(k): C_M vs Alpha

The goal was to achieve positively stable empty and loaded CG positions, so the team calculated the resulting moments of each force acting on the aircraft. A flat-plate airfoil was chosen for the stabilator to achieve the required level of pitching moment and negative slope for C_M versus Angle of Attack.

3.3.4 Fuselage

The first prototype was built with a single CF tube of 10mm diameter. This resulted in the severe cracks after multiple flight rounds due to the torsional load produced by the motor-propeller. Thus, we opted for a co-axial CF tube setup (**Section 3.1.2**) prototype 2 onwards while maintaining an FoS of 2.46. We used twill weave CF tubes as they provided 29.85% higher strength while only being 10.11% heavier than the single weave CF tubes. The primary length of the CF Tail Boom was derived by satisfying the required TMA, CG position, Avionics, and Payload

Plates placement. We chose top loading of payload plates into a basswood box between the wings as it provided fast and easy loading without the need for additional structure.

3.3.5 Landing Gears

The main landing gear passes through the carbon fiber spars and is mounted to the wing. This allows landing shocks to be transmitted directly to the CF spars and enabling the load to be distributed along the wingspan. The wing-mounted landing gear also provides adequate space for 3 boxes to be placed under the wing. Each side of the split main landing gear consists of two aluminum V-shaped arms that provide four contact points to the CF spars for better load distribution. The nose landing gear is a stainless-steel rod attached to the boom using a 3-D printed connector for on-ground maneuverability and strength to handle landing shocks.

3.3.6 Avionics

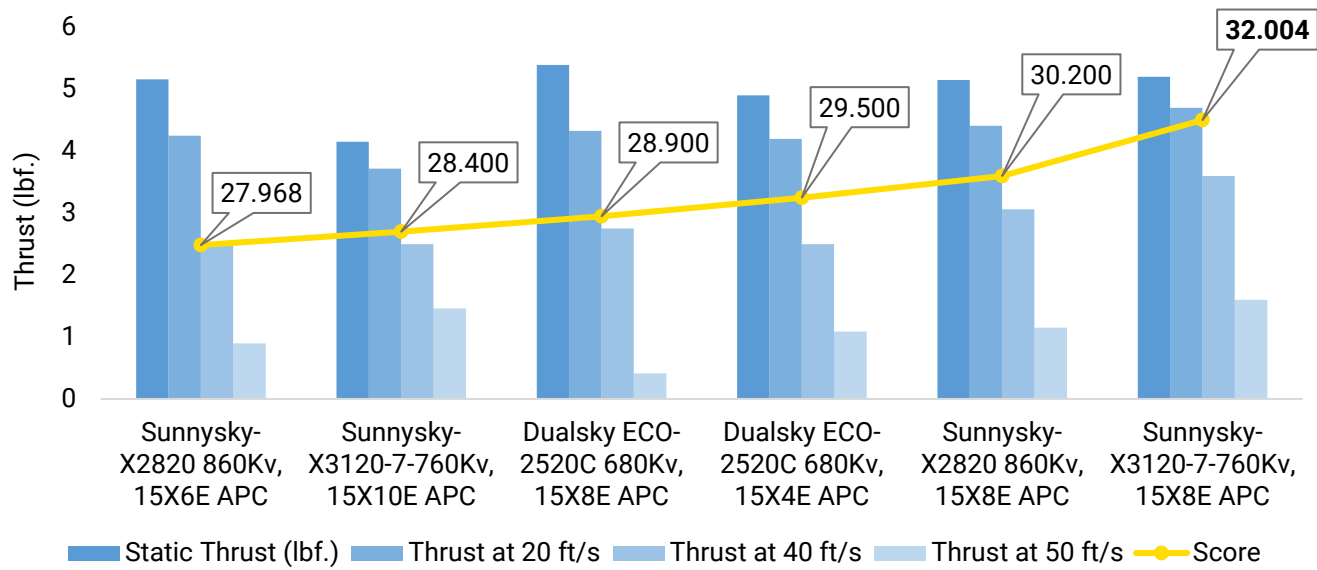
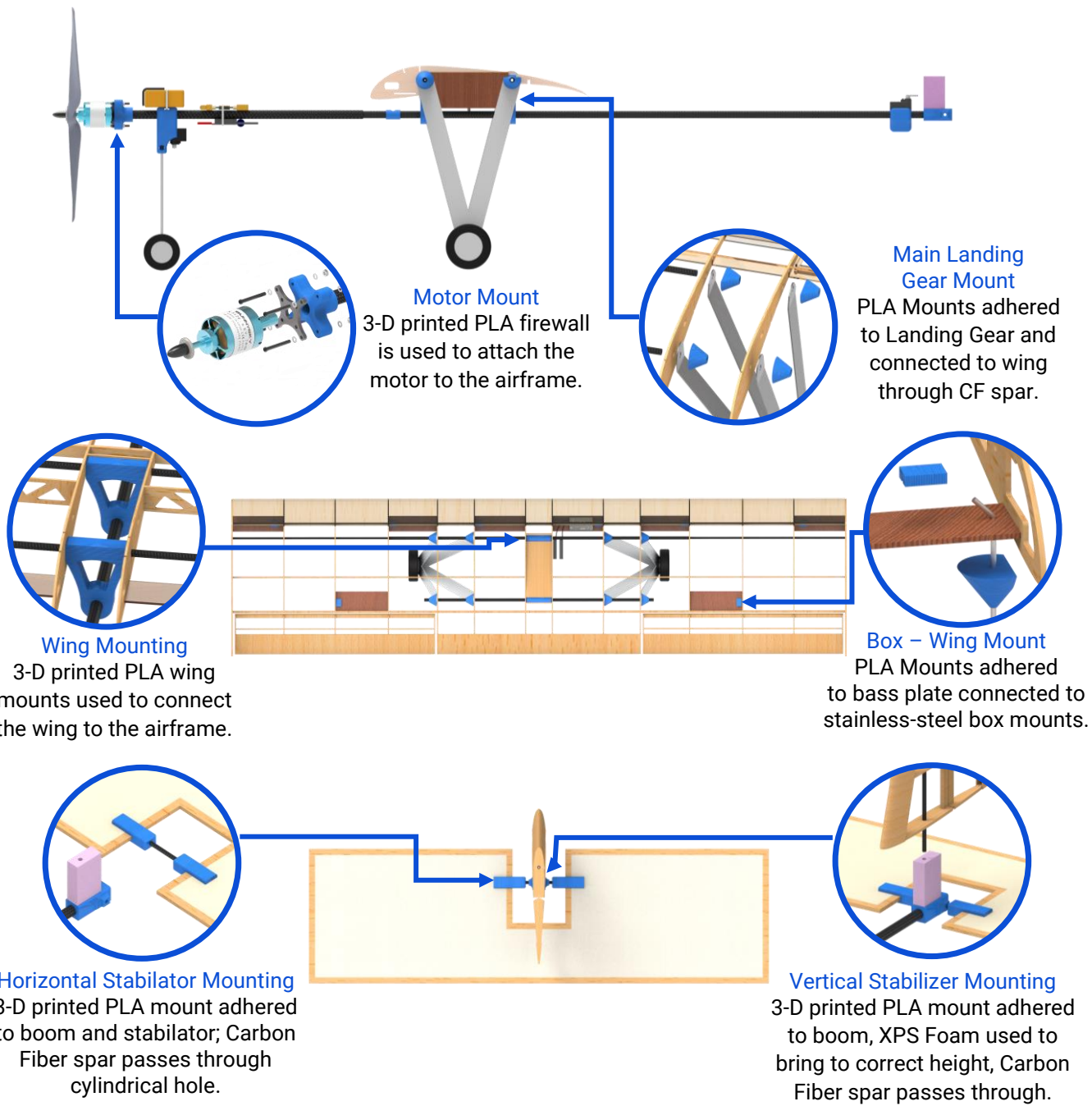


Figure 3(I): Motor-Propeller Combinations

The selection of motor and propeller was based on dynamic performance analysis for various flight conditions of take-off, turning and cruising. We shortlisted combinations, prioritizing dynamic performance. Our hypothesis was reinforced after extensive flight testing (**Section 5.3.2**), exhibiting motor-propeller combinations with superior dynamic performance outscoring their counterparts by virtue of higher speeds and reduced time taken to reach 300ft. We selected SunnySky X3120-7 760 Kv due to its overall higher dynamic thrust.

3.4 3-D Printed Interfaces and Attachments



4.0 Loads, Environments and Assumptions

4.1 Design Load Derivations

4.1.1 V-n Diagram

The V-n diagram is generated for empty and all-up weight of the aircraft. The load factor is nonzero when the aircraft is stationary due to the effect of propwash. Gust velocities of 5ft/s, 10ft/s and 15ft/s were also considered for the all-up weight load case.

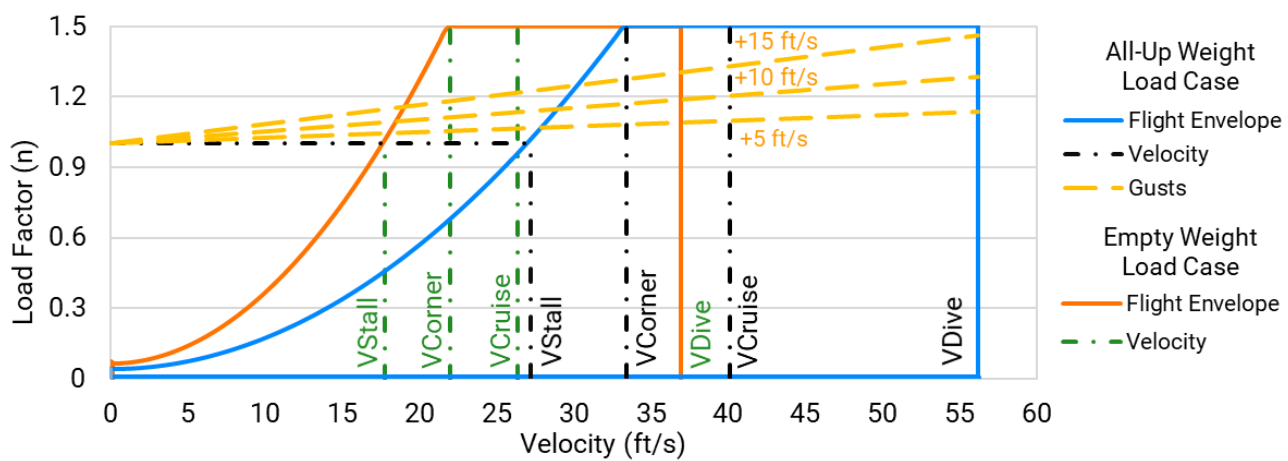


Figure 4(a): V-n Diagram

4.1.2 Landing Shocks

Sink Angle	Sink Rate (ft/s)	Impact Loading (lbf)
3°	0.9937	27.52549
5°	1.608	44.5416
10°	3.001	83.1277

Table 4(b): Landing Shock Calculations

The team calculated the impact loading on the airframe during touchdown for sink angles of 3°, 5° and 10° by calculating change in momentum and normal force. We used telemetry data to derive the former and calculate approach velocity. We recorded median impact time as 0.2 seconds from multiple flight tests. The main landing gear was designed with a FoS of 1.4 keeping these loads in mind.

4.2 Environmental Considerations

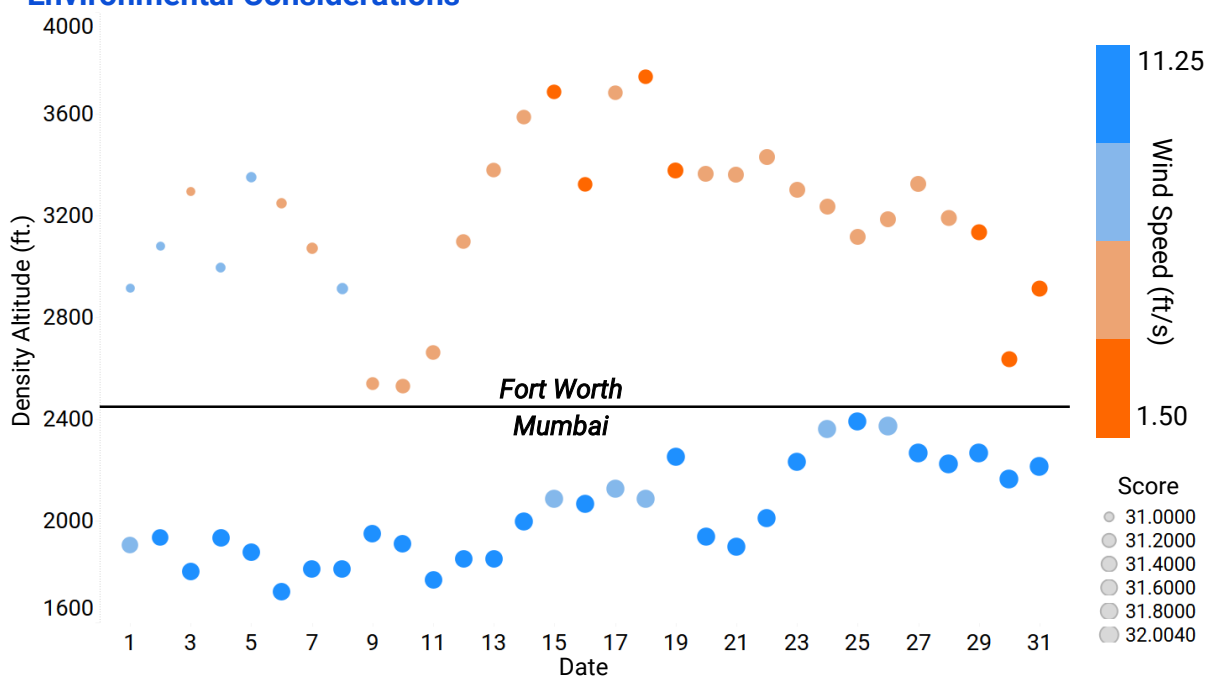


Figure 4(c): Environmental Considerations



We calculated the scores for the month of March for Mumbai and May for Fort Worth which were derived from the density altitudes. Historical data of various factors such as temperature, pressure, relative humidity, dew point, and altitude during the days of the competition as well as our testing period were accounted for. We also took into account differing values of rolling resistance at Mumbai and Fort Worth. The highest score obtained in Fort Worth is 31.653 points, with a decrease in score by 1.098% as compared to Mumbai.

5.0 Analyses

5.1 Analytical Tools

5.1.1 ANSYS & SolidWorks

The team used SolidWorks to perform low mesh CFD to find local maxima, whereafter ANSYS Fluent provided results on shortlisted planforms using high element quality mesh to find the global maxima. ANSYS Mechanical was used for Finite Element Analysis (FEA) of load-bearing components. Topology Optimization and Response Surface techniques on ANSYS were used to reduce the weight of structures, while varying several geometric parameters, but still be within MoS. SolidWorks was also used for high accuracy balancing of masses and CG.

5.1.2 XFLR5 & MATLAB

We used XFLR5 to interpolate airfoils and export their polars. It was also used for obtaining and analyzing static and dynamic stability eigenvalues (**Section 5.3.4**). Tornado VLM in MATLAB was used for analyses of airfoils to obtain C_L and C_D values. The Global Optimization Toolbox by MathWorks was used to optimize the above system variables using the advanced technique of genetic optimization to find global maxima with the score being the fitness function.

5.1.3 Tableau & Microsoft Excel

They are used to generate detailed and efficient graphs and plots with varying scores, wingspan, cargo configurations, ARs, time, and payload showing how we optimized those parameters.



5.2 Developed Models

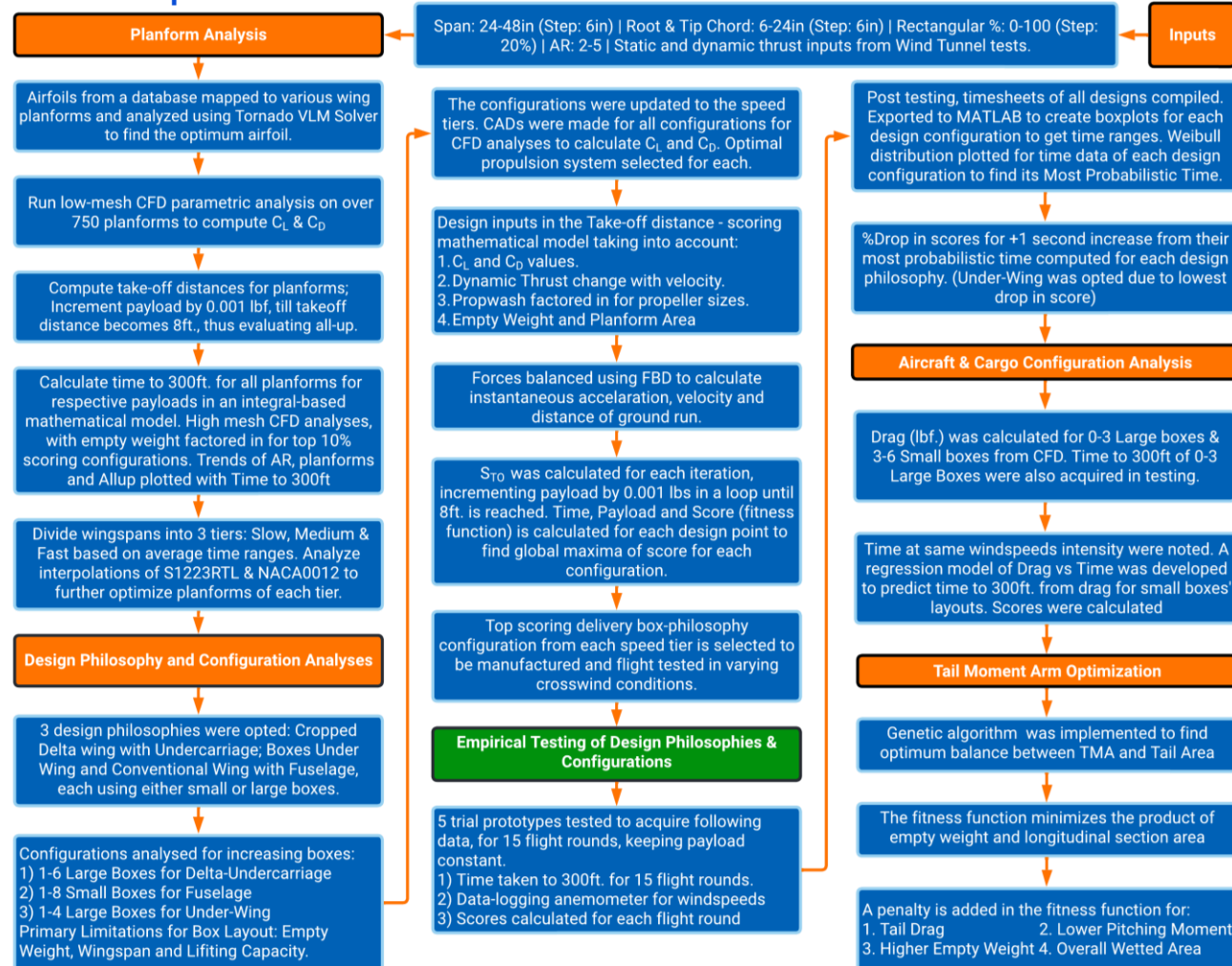


Chart 5(a): Developed Models

5.3 Performance Analyses

5.3.1 Dynamic Thrust Performance

We analyzed dynamic thrust characteristics of various motor-propeller combinations (Section 3.3.6) using the wind tunnel setup as described in Section 6.0. Figure 5(b) compares the values of three best combinations after curve fitting data showing payload lifted vs take-off distance.

Dynamic thrust was prioritized over high static thrust allowing for flight in intense headwinds.

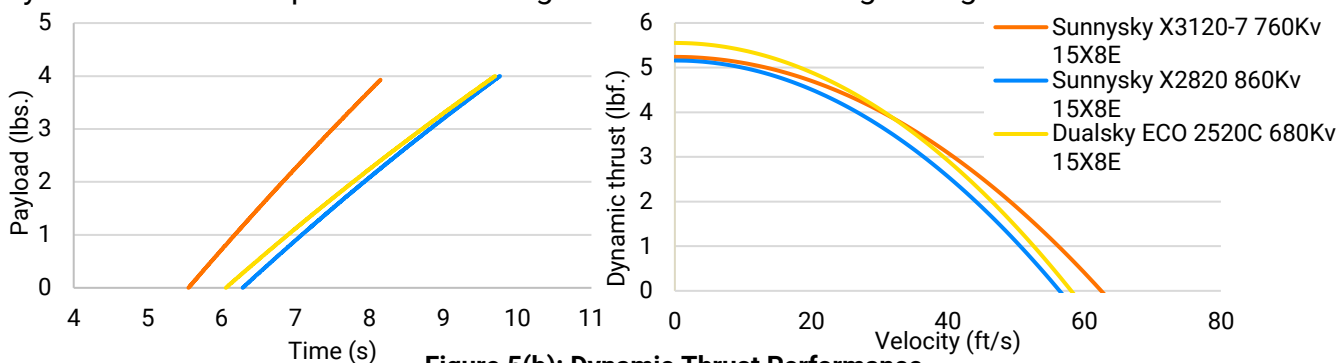


Figure 5(b): Dynamic Thrust Performance

5.3.2 Take-off and Climb Out Performance

We incorporated equations governing take-off in our model, running simulations for each iteration of our aircraft. Below are the flight trajectories of our prototypes derived from telemetry after empirical testing with a prototype summary. The 4th prototype attained the take-off velocity quicker, gained altitude with relative ease and followed a smoother trajectory as compared to earlier iterations. Relevant climb rates and altitude gain for the prototypes have been illustrated.

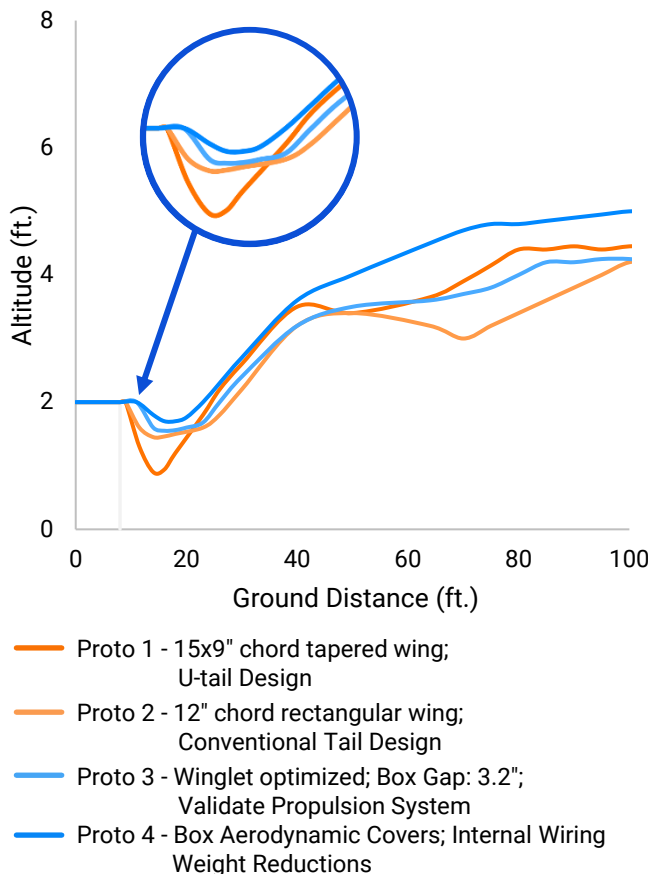


Figure 5(c): Take-off and Climb-out Telemetry

Prototype (Score-Time to 300ft)	Pros	Cons	To improve/test
1 (27.517 - 8.6 sec)	Payload 2.5 lbs. Dynamically Stable; Apt CG.	Less lift; Overcompensated yawing moments	Wing planform; Reduce vertical tail area
2 (28.596 - 8.6 sec)	Payload 2.7 lbs.; Lift increased due to increase in planform area.	Aileron effectiveness suboptimal; High torsion loads on CF Boom	Propulsion system; Twill weave CF Boom; Aileron effectiveness
3 (30.708 - 8.3 sec)	Payload 2.9 lbs.; Increased lift and aileron effectiveness	High drag produced; High empty weight and FoS.	Aerodynamic box covers. Perform weight reductions.
4 (32.004 - 8.1 sec)	Payload 3 lbs.; Reduced box drag by 55.4%; Smoother trajectory	Maxima of payload-time limit reached	Final configuration set to 3lbs. & 3 Large boxes.

Table 5(d): Post Flight-Test Optimizations

5.3.3 Flight and Maneuver Performance

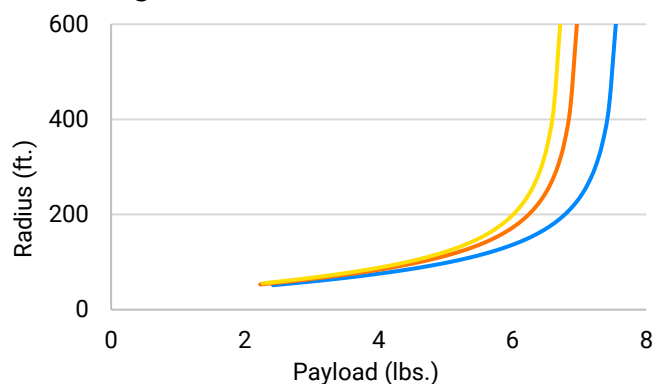


Figure 5(e): Minimum Turning Radius

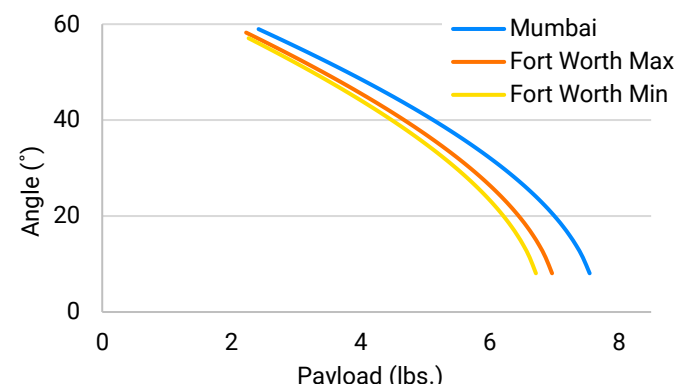


Figure 5(f): Maximum Banking Angle



The team calculated the maximum banking angles and turning radii for various load factors and velocities; by resolving the forces acting on the free-body diagram of the aircraft. The graphs represent variations in these factors depending on air densities at their respective locations.

5.3.4 Static and Dynamic Stability

The negative slope of C_M vs Angle of Attack (**Figure 3(k)**) indicates that the aircraft is statically stable. The neutral point is 19.47" from the aircraft datum and the static margin is 6.10% of Mean Aerodynamic Chord.

Oscillating Aircraft Dynamic Response		
Aircraft motion	Damping Factor	Oscillation Time (seconds)
Short Period (Longitudinal)	0.690	0.993
Phugoid (Longitudinal)	0.021	7.634
Dutch Roll (Lateral)	0.268	1.339
Non-oscillating Aircraft Dynamic Response		
Roll Dampening (Lateral)	Tau: 0.010	Dampening Time: 0.007 seconds
Spiral Instability (Lateral)	Pilot Response Time: 1.8 seconds	Pitch at Response Time: 58.777 °/s

Table 5(g): Stability Response

Dynamic stability was assured through analyses and empirical testing in varying conditions. We ensured FoS of 1.2 on all control surfaces allowing for the aircraft to be controllable in all axes.

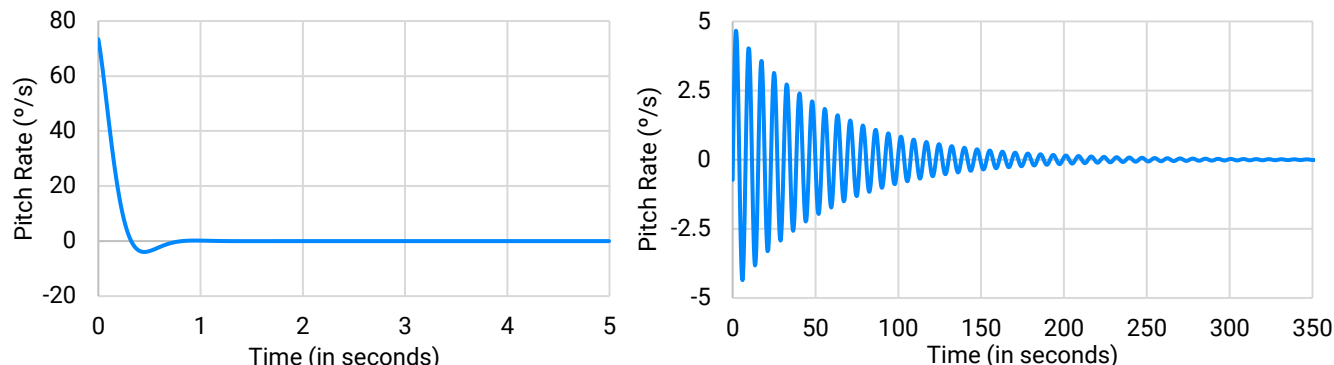


Figure 5(h): Short Period and Phugoid Modes

Roll Dampening	-97.7134	Dutch Roll	-1.30848+4.69662i	Spiral Instability	0.3798
----------------	----------	------------	-------------------	--------------------	--------

Table 5(i): Lateral Stability Eigenvalues

5.3.5 Aircraft Performance Prediction

Plots were generated by resolving forces and integrating the resultant the resultant differential equations on MATLAB considering parameters like predicted winds of 2.93 ft/s, rolling drag, inertia, dynamic thrust, and variation in lift and drag due to boxes under the wings. The predicted

performance was plotted (Appendix B) for payload of 3 lbs. and 3 large delivery boxes.

5.3.6 Drag Polar Analysis

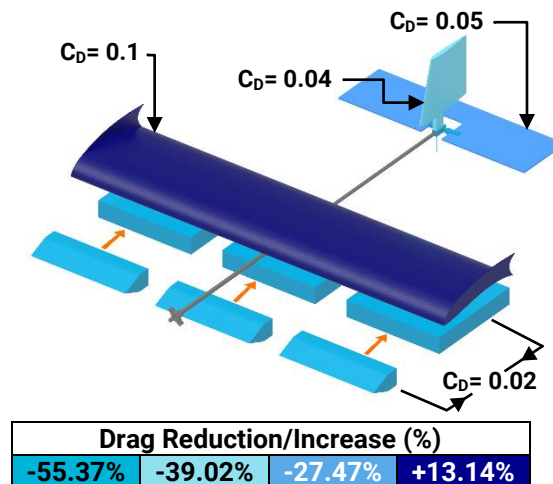


Figure 5(j): Drag Polar Analysis

We calculated percentage drag contributions of major components of the aircraft over the prototypes. The change from U-tail to inverted T-tail, led to a significant decrease in drag. Aerodynamic Box covers reduced C_D of boxes by 0.02. An increase in the wing area led to an increase in drag. The net reduction in drag over all prototypes was 43.42%.

5.4 Structural Analysis

5.4.1 Critical Margins

Material	Component/Condition	Max Stress Induced (PSI)	Max Allowed Stress (PSI)	FoS
Balsa	Wing Airfoils	1121.86	1914.5	1.707
Basswood	Payload Mount during cruise	1627.38	2164.1	1.330
	Payload Mount while turning	1718.48	2164.1	1.259
Carbon Fiber	Tail Boom during cruise	7108.27	18606.89	2.618
	Tail Boom while turning	7550.6	18606.89	2.464
PLA	3D Printed Attachments during cruise	5181.2	8777.25	1.694
	3D Printed Attachments while turning	5622.61	8777.25	1.561
5052 Aluminum	Main Landing Gear during landing	9283.82	13053.42	1.406
XPS Foam	Horizontal Stabilizer during turning	205.23	290.55	1.416

Table 5(k): Material Analysis

5.4.2 Applied Loads and Material Selection

1) Tail Force Analysis

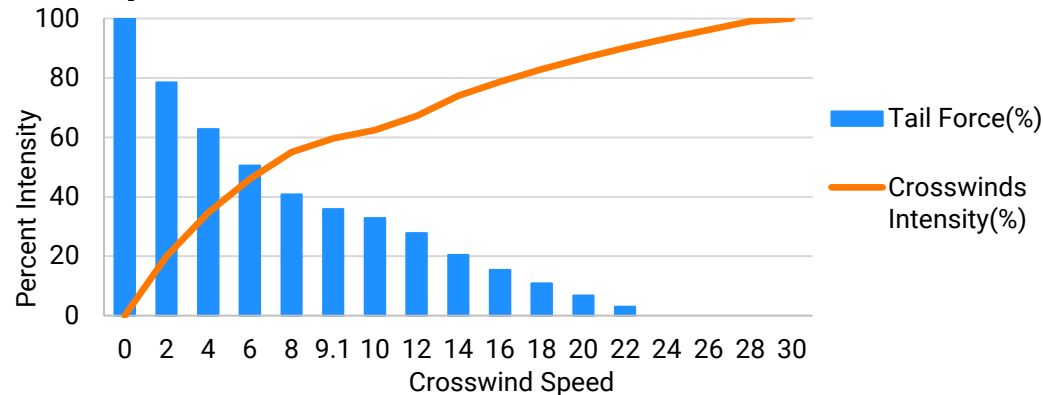


Figure 5(l): Crosswind Analysis

The team analyzed rudder effectiveness in crosswind conditions by developing a mathematical model where rudder forces were measured at varying crosswind intensities for in-flight



conditions. The rudder becomes ineffective at crosswind velocity of 24.0ft/s. Since Fort Worth has maximum winds of 9.1ft/s, according to past data, rudder performs at 35.81% effectiveness.

2) Material Selection

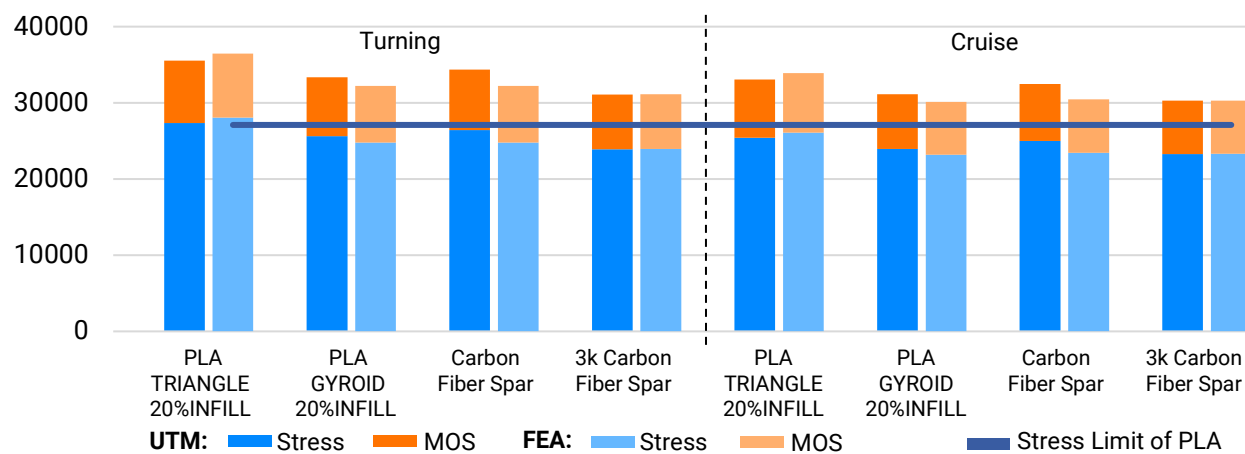


Figure 5(m): Composite Stress Analysis

We constructed the airframe primarily with carbon fiber for its high strength to weight ratio (S/W) ratio and stiffness. Balsa and XPS were used in the wing & vertical tail and stabilator, respectively, for their low density and high S/W ratio. We used basswood for the payload bay assembly due to concentrated loads. PLA 3-D printed mounts were used at junctions and interfaces for ease of manufacturing, and ability to optimize infill density and pattern.

3) Mass Properties and Balance

A. Weight Distribution

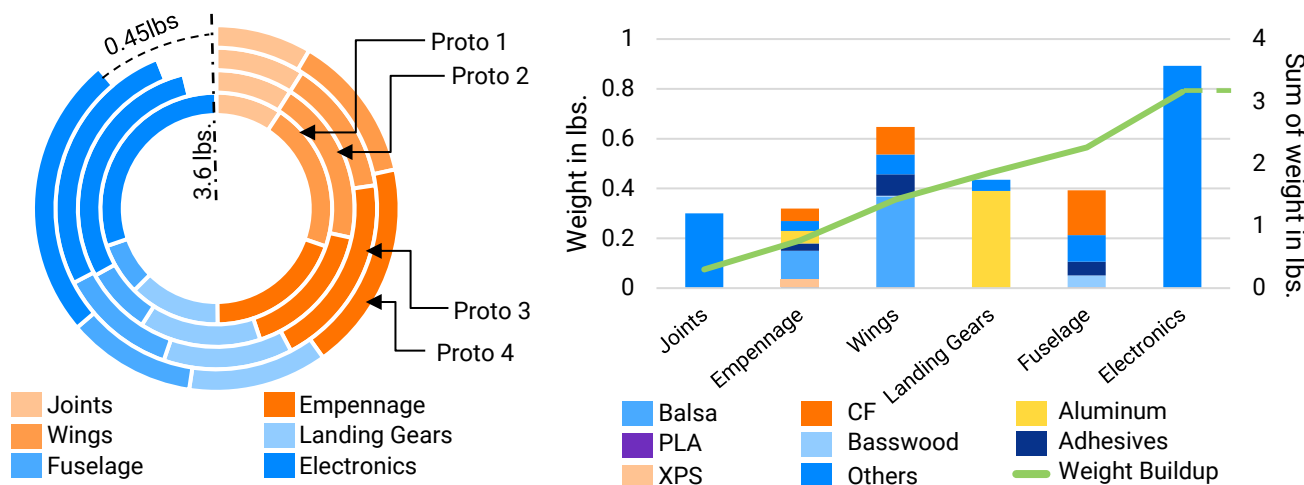


Figure 5(n): Weight Buildup

Weight reduction techniques were performed on components with lesser critical loading while reinforcing regions requiring a high FoS. Empty weight was reduced with each iteration.

B. Center of Gravity

Based on our calculations and pilot inputs, the aircraft was designed with the CG 1.06" in front of the Neutral Point ensuring static stability. The main landing gear was placed near the CG to aid in equal weight distribution and prevent excessive loading on the nose landing gear.

6.0 Sub-Assembly Tests and Integration

6.1 Propulsion System and Testing

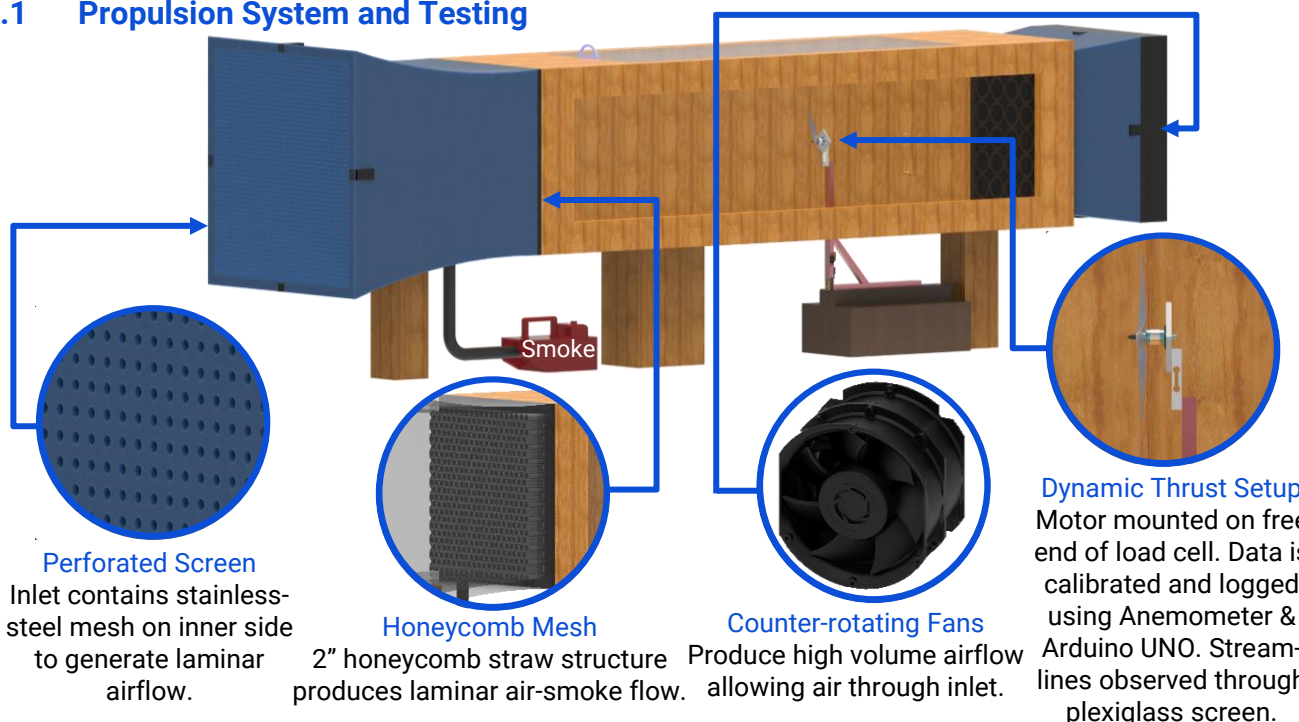


Figure 6(a): Novel Wind Tunnel Setup

The team shortlisted motors-propeller combinations after comparing thrust values from eCalc, limiting them to 450W. We measured dynamic thrust using a wind tunnel (**Figure 6(a)**) having counter rotating fans at the outlet and a honeycomb mesh & stainless-steel mesh in contraction cone. The median error for thrust values was found to be 2.91%, when compared to online tools.

6.2 Battery and Servo Testing

Battery endurance was tested during multiple flight tests for 2 complete flight rounds.

Control Surface	Servomotor	Rated Torque (oz-in)	Control Surface Deflection	Required Torque (oz-in)
Aileron	Turnigy XGD-11HMB	268.01	30°	37.51
Stabilator	Turnigy TGY-813	124.98	30°	52.1
Rudder	Turnigy XGD-11HMB	268.01	30°	31.6
Nose Landing Gear (Steering)	Turnigy TGY-9018MG	319.410	30°	183.52

Table 6(b): Servo Torque Requirements



6.3 Flight Testing

We tested various design configurations equipped with anemometer, accelerometer, pitot tube, GPS sensor and altimeter to gather telemetry data. We conducted flights with an incremental weight build-up strategy and compared analytical values with post flight empirical values.

7.0 Manufacturing

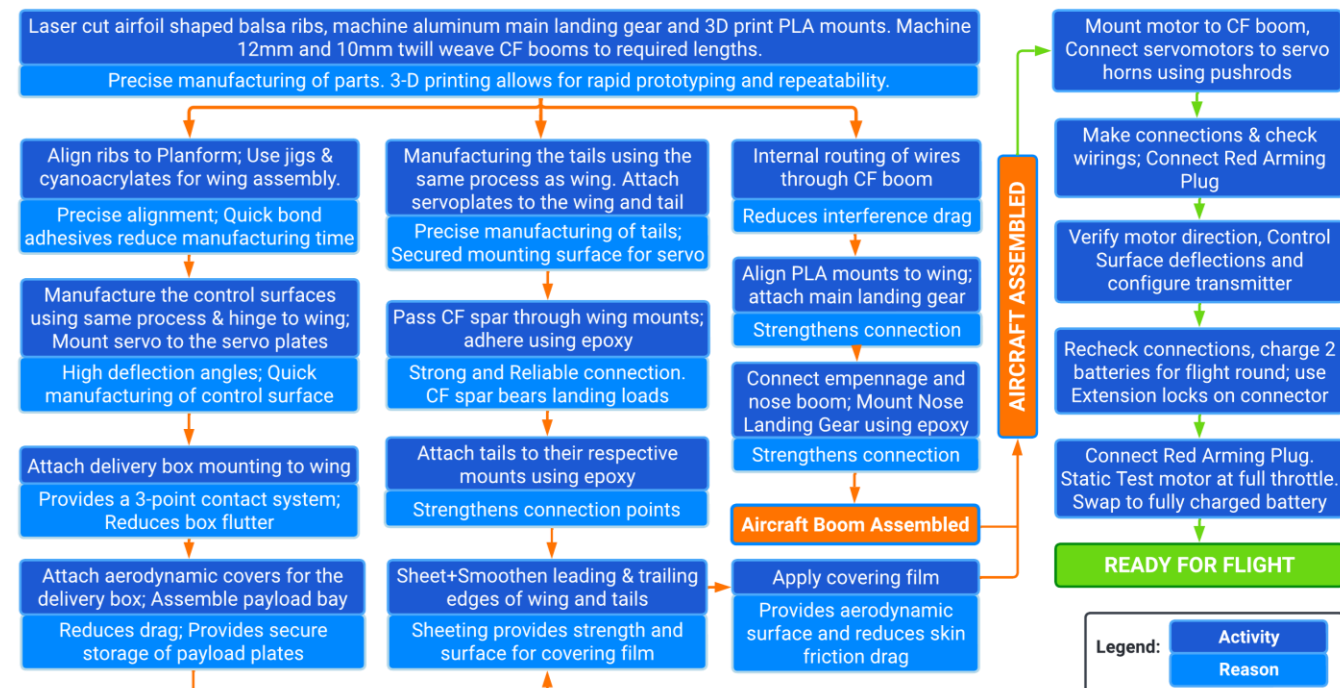


Chart 7(a): Manufacturing Process

8.0 Conclusion

The designed aircraft can carry 3lbs. of payload plates and 3 large boxes to 300ft. in 8.1 seconds with the unique combinations of materials used ensuring structural soundness and extensive empirical testing backing our calculations. Despite the challenges faced, we hope to make the most of the opportunity and expect to be competitive at SAE Aero Design East, 2022.

Table of References:

1. Anderson, John D., "Introduction to Flight: Its Engineering and History"
2. Caughey, David A., "Introduction to Aircraft Stability and Control Course Notes"
3. Nicolai, Leland M., and Grant Carichner., "Aircraft Design"
4. Sadraey, Mohammad H., "Aircraft Design: A Systems Engineering Approach"
5. Team 314, DJS Skylark – Micro Class Design Report, SAE Aero Design Knowledge, 2021.



Appendix A – Backup Calculations

Take-off Equation: (SECTION 5.3.2)

$$S_{TO} = \frac{1}{2B} \ln \left| \frac{A}{A - BV_{TO}^2} \right| ; \text{ Where, } A = \left(\frac{T_s}{W} - \mu \right) ; B = \frac{g}{\omega} \left[\frac{1}{2} \rho A (C_D - \mu C_L) + a \right] ; a = 0.11126$$

Time: (SECTION 5.2)

$$t_2 - t_1 = \frac{1}{2\sqrt{MN}} \left\{ \left[\ln \frac{\sqrt{M} + V_2 \sqrt{N}}{\sqrt{M} - V_2 \sqrt{N}} \right] - \left[\ln \frac{\sqrt{M} + V_1 \sqrt{N}}{\sqrt{M} - V_1 \sqrt{N}} \right] \right\} ; \text{ Where, } M = \left(\frac{T_0}{W} \right) ; N = \left[\frac{g}{\omega} \left\{ \frac{1}{2} \rho A C_D + a \right\} \right]$$

Where, t_1 = Initial time, t_2 = Final time, V_1 = Initial velocity, V_2 = Final velocity, ρ = Density

Servo Torque Calculations: (SECTION 6.2)

$$\text{Servo Torque Required} = (8.5 \times 10^{-6}) \frac{C^2 \times v_d^2 \times \text{control surface span} \times \sin^2(S_1)}{\cos(S_1) \times \tan(S_2)} \times \frac{\text{control horn height}}{\text{servo arm length}}$$

Gust Induced Load factor: (SECTION 4.1.1) Turning Radius Calculations: (SECTION 5.3.3)

$$n = 1 + \frac{k_g V_g E V_E \alpha \rho S}{2mg} ; g = 9.80665 \text{ m/s}^2 \quad \text{Radius} = \frac{mv^2}{L \sin \phi} ; \text{Banking Angle, } \phi = \cos^{-1} \left(\frac{W}{L} \right)$$

Drag Polar: (SECTION 5.3.6)

$$C_D = C_{D0} + C_{Di} ; C_{Di} = C_L^2 / (\pi \times AR \times e) ; C_{D0} = C_{D0(\text{fuse})} + C_{D0(\text{wing})} + C_{D0(\text{Hstab})} + C_{D0(\text{Vstab})}$$

$$C_{D\text{minimum(surface)}} = C_{f(\text{surface})} \times \text{Form Factor}_{(\text{surface})} \times \frac{\text{wetted area}}{\text{reference area}} ; \text{ Where, } e = \text{Efficiency Factor}$$

Climb Out: (SECTION 5.3.2)

$$\theta = \cos^{-1} \left(\frac{0.5 \rho C_L S v^2}{mg} \right) ; v_y = v_x \tan \theta ; v = (v_x^2 + v_y^2)^{0.5} ; \text{ Where, } \theta = \text{climb angle}$$

Stability Equations: (SECTION 5.3.4)

$$\text{Equilibrium condition: } C_{Mo} + C_L(h - h_o) - C_{LT} * \bar{V} = 0 ; \text{ Where, } C_{Mo}, C_{LT} = \text{Coefficient}$$

$$\text{of moment of wing and lift of tail} \\ \text{For negative slope of } C_M \text{ vs } \alpha: \frac{\delta C_m}{\delta \alpha} = 0 + \frac{\delta C_L}{\delta \alpha} (h - h_o) - \frac{\delta C_{LT}}{\delta \alpha} * \bar{V}$$

$$\text{For Neutral Point: } \frac{\delta C_L}{\delta \alpha} (h_n - h_o) = \frac{\delta C_{LT}}{\delta \alpha} * \bar{V}$$

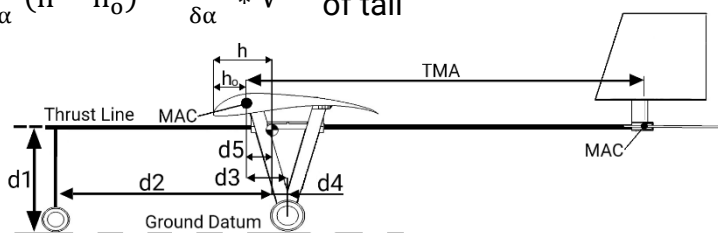
Moment Equations: (SECTION 5.3.4)

$$\text{On-ground } T_s d_1 - W d_2 \leq 0$$

$$\text{Take-off } T_d d_1 - L_{W_1} d_3 + W d_4 - L_{T_1} (TMA - d_3) = 0$$

$$\text{In flight } L_{W_2} d_5 = L_{T_2} (TMA + d_5)$$

$$\text{Where } L_{W_1} \& L_{W_2} = \text{Lift of Wing - take-off \& in-flight} \\ L_{T_1} \& L_{T_2} = \text{Lift of Tail - take-off \& in-flight}$$





Appendix B – Technical Data Sheet

Aircraft Performance Prediction (Micro Class)

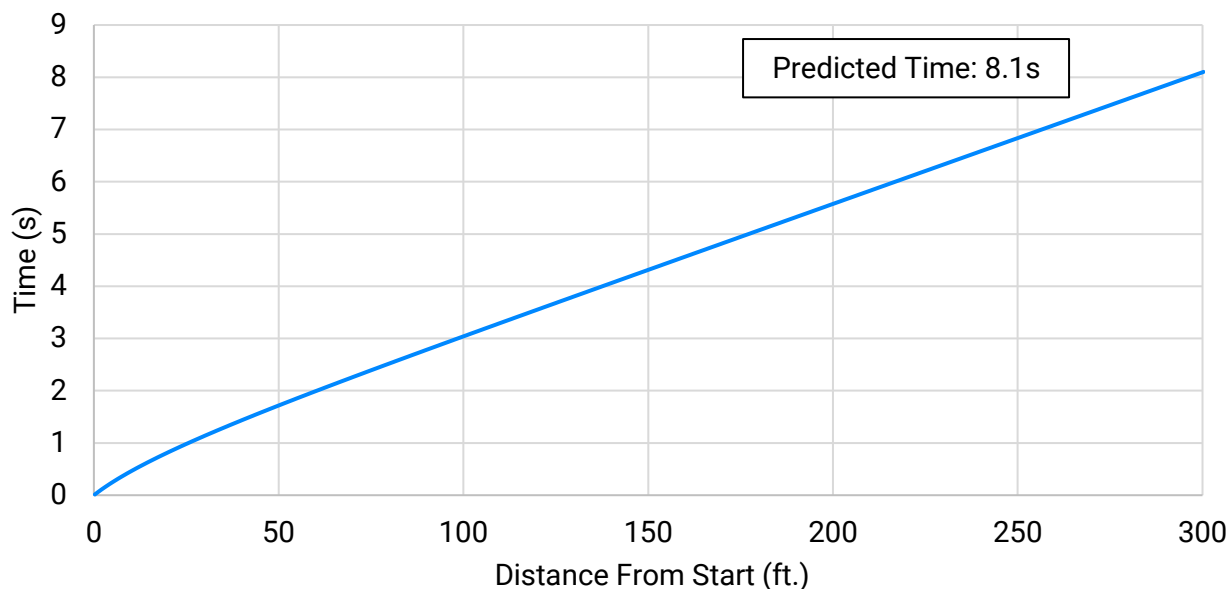
Team Name: DJS Skylark – MICRO CLASS

Team Number: 311

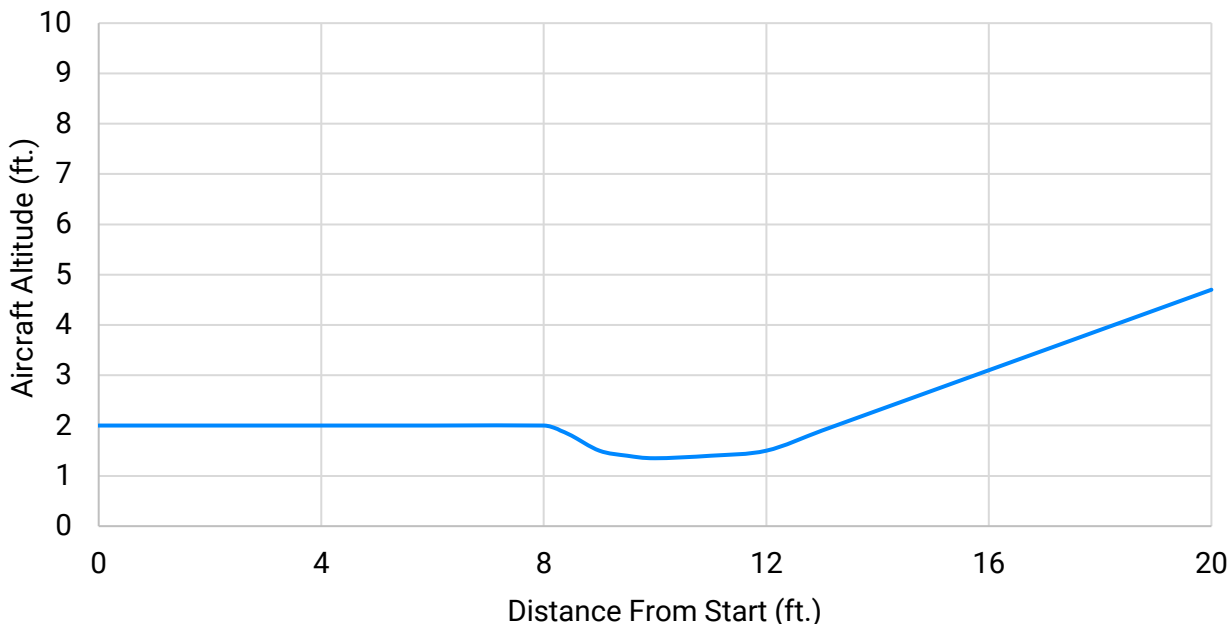
School Name: Dwarkadas J. Sanghvi College of Engineering

Payload Combination Analyzed: 3 Large Boxes + 3 lbs. Payload

Time vs Ground Distance



Altitude vs Ground Distance



AIRCRAFT SUMMARY DATA

WINGSPAN	MAC	TMA	EMPTY WEIGHT	BATTERY	MOTOR MODEL	MOTOR KV	PROPELLER	SERVO (Nose Landing Gear) (A)	SERVO (Aileron) (B)	SERVO (Stabilator) (C)	SERVO (Rudder) (E)
48 ± 0.1"	12.00"	28.6±0.1"	3.150 lbs	Dinogy LiPO 850mAh 4S	SunnySky X3120-7 -14 poles	760Kv	APC 15x8E	Turnigy TGY-9018MG (319.40oz-in)	Turnigy XGD-11HMB (268.00 oz-in)	Turnigy TGY-813 (124.98oz-in)	Turnigy XGD-11HMB (268.40 oz-in)

